Splines computation by subdivision and sample rate conversion

Amir Z. Averbuch[1]*, Pekka Neittaanmäki[2], Gil Shabat[3], Valery A. Zheludev[1]

[1]School of Computer Science, Tel Aviv University, Tel Aviv 69978, Israel

[2]Department of Mathematical Information Technology, University of Jyväskylä, Finland

[3]School of Electrical Engineering, Tel Aviv University, Tel Aviv 69978, Israel

Abstract

We present algorithms for explicit computation of one- and multi-dimensional periodic splines of arbitrary order at triadic rational points and of splines of even order at dyadic rational points. These algorithms use the direct and the inverse Fast Fourier transform (FFT) and the implementation is as fast as the FFT. The algorithms are based on dyadic and triadic subdivision of splines. Interpolating and smoothing splines are used for sample rate conversion such as upsampling of discrete-time signals and digital images, which may be contaminated by noise. The performance of the spline based rate conversion is compared with the performance of the prolate spheroidal wave functions based rate conversion.

Key words: Periodic splines, subdivision, interpolating splines, smoothing splines,sample rate conversion, prolate spheroidal wave functions

1 Introduction

Splines are an important tool in approximation theory, computer aided geometric design and signal/image processing. Splines have been designed by their samples at grid points. An important problem is how to design explicitly splines of any order and how to achieve fast calculation of their values at internal points between grid points. In the paper, we propose a fast and efficient scheme for computation of one- and multi-dimensional periodic splines of any order at triadic rational points and of splines of even order at dyadic rational points starting from their samples at equidistant grid points. The idea behind the dyadic algorithm is the following. The spline $S(t)$, which interpolates available grid samples $S(k)$, is designed and its midpoints values between grid points are explicitly calculated. The newly derived samples are interpolated by the new spline whose midpoint values are calculated, then, the process is iterated. We prove that if the spline order is even then the scheme at each step generates values of the initial spline. Thus, after m iterations the values $S(k/2^m)$ are derived. The calculations are reduced to those that come from the application of one direct and one inverse FFT independently of the number of iterations. This is not true for the odd order

*Amir Averbuch, Tel: +972-54-5694455, Fax: +972-3-6422020, Email address: amir@math.tau.ac.il

splines. However, if, instead of $S(k/2)$ values, the triadic values $S(k/3)$ and $S(2k/3)$ are calculated, then the scheme becomes applicable to splines of any order. Extension of the algorithms to multidimensional splines is straightforward.

A natural application of these spline algorithms is restoration and rate conversion to many sample rates such as upsampling of signals/images. A spline is designed, which interpolates the available samples or pixels then the object is upsampled by introducing intermediate spline values. When the available data is contaminated by noise then the so-called smoothing splines are used for efficient processing. The performances of upsampling by splines are compared to the performances of the prolate spheroidal wave functions.

The paper is organized as follows. Section 2 provides some preliminaries on the interpolatory subdivision and periodic splines. In particular, interpolating and smoothing splines of any order are designed in one and two dimensions and some of their properties are established. In Section 3, the dyadic subdivision for periodic splines is presented, which leads to computation of periodic splines at dyadic rational points. Section 4 does the same for the triadic subdivision schemes. In Section 5, a few examples of application of the designed splines to upsampling of signals and images are given. Their performances are compared with the performance of prolate spheroidal wave functions.

2 Preliminaries

Throughout the paper, we denote $N = 2^j$, $N_m = 2^m N = 2^{j+m}$, $N_{\tilde{m}} = 3^m N$, $m \in \mathbb{N}$, $\omega = e^{2\pi i/N}$. The space of N-periodic discrete-time signals is denoted by $\Pi[N]$. The spaces of N_m-periodic and $N_{\tilde{m}}$-periodic signals are denoted as $\Pi[N_m]$ and $\Pi[N_{\tilde{m}}]$, respectively. The direct and inverse discrete Fourier transform (DFT) of a signal $\mathbf{x} = \{x[k]\} \in \Pi[N_m]$ are

$$\hat{x}[n]_m = \sum_{k=0}^{N_m-1} \omega^{-2^{-m}kn}\, x[k], \quad x[k] = \frac{1}{N_m} \sum_{n=0}^{N_m-1} \omega^{2^{-m}kn}\, \hat{x}[n]_m.$$

If $\mathbf{x} \in \Pi[N_{\tilde{m}}]$ then its DFT and IDFT are

$$\hat{x}[n]_{\tilde{m}} = \sum_{k=0}^{N_{\tilde{m}}-1} \omega^{-3^{-m}kn}\, x[k], \quad x[k] = \frac{1}{N_{\tilde{m}}} \sum_{n=0}^{N_{\tilde{m}}-1} \omega^{3^{-m}kn}\, \hat{x}[n]_{\tilde{m}}.$$

We retain for N-periodic signals ($m = 0$) the standard notation $\hat{x}[n] = \hat{x}[n]_0$.

The inner product and the norm in the space $\Pi[N_m]$ are defined as

$$\langle \mathbf{x}, \mathbf{y} \rangle \triangleq \sum_{k=0}^{N_m-1} x[k]\, y^*[k] = \frac{1}{N_m} \sum_{n=0}^{N_m-1} \hat{x}[n]_m\, \hat{y}[n]_m^*, \quad \|\mathbf{x}\|^2 \triangleq \sum_{k=0}^{N_m-1} |x[k]|^2 = \frac{1}{N_m} \sum_{n=0}^{N_m-1} |\hat{x}[n]_m|^2$$

and similarly in the space $\Pi[N_{\tilde{m}}]$. Here, $\cdot^*$ means complex conjugation.

2.1 Interpolatory subdivision

Interpolatory subdivision schemes (ISS) are refinement rules, which iteratively refine the data by inserting values that correspond to intermediate points, using linear combinations of values in initial points while the

data in these initial points are retained. Non-interpolatory schemes also update the initial data in addition to the insertion of values into intermediate points. Stationary schemes use the same insertion rule at each refinement step. A scheme is called uniform if its insertion rule does not depend on the location in the data.

To be more specific, a univariate stationary uniform subdivision scheme with binary refinement ([9, 8, 23]) $\mathfrak{S}_a^2$ consists of the following: A function $F(t)$, which is defined on the grid $\mathbf{g}^m = \{k/2^m\}_{k\in\mathbb{Z}}$: $F(k/2^m) = f^m[k]$, is extended onto the grid $\mathbf{g}^{m+1}$ by filtering the upsampled array

$$(\uparrow 2)\mathbf{f}^m = \{\breve{f}^m[k]\}, \quad \breve{f}^m[k] = \begin{cases} f^m[l], & \text{if } k = 2l; \\ 0, & \text{otherwise,} \end{cases}$$

by an interpolating filter $\mathbf{a} = \{a[k]\}_{k\in\mathbb{Z}}$ such that $a[2k] = \delta[k]$. Thus, one dyadic refinement step is

$$F(k/2^{m+1}) = f^{m+1}[k] = \sum_{l\in\mathbb{Z}} a[k-2l]f^m[l] \tag{2.1}$$

$$\Longleftrightarrow \begin{cases} f^{m+1}[2k] = f^m[k], \\ f^{m+1}[2k+1] = \sum_{l\in\mathbb{Z}} a[2(k-l)+1]f^m[l]. \end{cases}$$

The next refinement step employs $\mathbf{f}^{m+1}$ as an initial data. The filter $\mathbf{a} = \{a[k]\}_{k\in\mathbb{Z}}$ is called the refinement mask of $\mathfrak{S}_a^2$.

A subdivision scheme with ternary refinement ([12, 11, 5]) $\mathfrak{S}_a^3$ consists of the following: A function $F(t)$ such that $F(k/3^m) = f^m[k]$, which is defined on the grid $\mathbf{g}^m = \{k/3^m\}_{k\in\mathbb{Z}}$, is extended onto the grid $\mathbf{g}^{m+1}$ by filtering the upsampled array

$$(\uparrow 3)\mathbf{f}^m = \{\breve{f}^m[k]\}, \quad \breve{f}^m[k] = \begin{cases} f^m[l], & \text{if } k = 3l; \\ 0, & \text{otherwise.} \end{cases}$$

Thus, one triadic refinement step is

$$F(k/3^{m+1}) = f^{m+1}[k] = \sum_{l\in\mathbb{Z}} a[k-3l]f^m[l] \tag{2.2}$$

$$\Longleftrightarrow \begin{cases} f^{m+1}[3k] = f^m[k], \\ f^{m+1}[3k\pm 1] = \sum_{l\in\mathbb{Z}} a[3(k-l)\pm 1]f^m[l]. \end{cases}$$

Next, the refinement step employs $\mathbf{f}^{m+1}$ as an initial data.

In the paper we assume that the initial data array $\mathbf{f}^0$ is N-periodic (belongs to $\Pi[N]$). Consequently, the refined data arrays $\mathbf{f}^m \in \Pi[N_m]$ for the scheme $\mathfrak{S}_a^2$ and $\mathbf{f}^m \in \Pi[N_{\tilde{m}}]$ for the scheme $\mathfrak{S}_a^3$. In the periodic setting, filtering a signal $\mathbf{x} \in \Pi[N_{\tilde{m}}]$ is interpreted as a discrete circular convolution of the signal with a signal $\mathbf{a}_{\tilde{m}} \in \Pi[N_{\tilde{m}}]$: $\mathbf{y} = \mathbf{a}_{\tilde{m}}\,\mathbf{x} \Longleftrightarrow y[k] = \sum_{l=0}^{N_{\tilde{m}}-1} a_{\tilde{m}}[k-l]\,x[l]$. Similarly, it holds for the signals from $\Pi[N_m]$. We call $\mathbf{a}_{\tilde{m}}$ and $\mathbf{a}_m$ the p-filters.

2.2 Space of periodic splines

Definition 2.1 *An* N*-periodic function $S^p(t)$ is called the periodic spline of order $p \in \mathbb{N}$ on the grid $\{k\}$, $k \in \mathbb{Z}$, if it has $p-2$ continuous derivatives (belongs to C^{p-2}) and consists of pieces of polynomials of degree*

$p-1$ that are linked to each other at the nodes. Nodes of splines of even and of odd orders are located at the points $\{k\}$ and $\{(k+1)/2\}$, $k \in \mathbb{Z}$, respectively.

The space of N-periodic splines of order p is denoted as ${}^p\mathcal{S}$. A widely used basis of the space ${}^p\mathcal{S}$ consists of the shifts of the so-called B-splines.

2.2.1 Periodic B-splines

Let $N = 2^j,\ j \in \mathbb{N}$. The centered N-periodic B-spline $B^1(t)$ of first order on the grid $\{k\},\ k \in \mathbb{Z}$, is defined via periodization of the characteristic function $\chi[-1/2, 1/2](t)$ of the interval $(-1/2, 1/2)$ such that

$$\chi[a,b](t) \triangleq \begin{cases} 1, & t \in (a,b); \\ 0, & \text{otherwise}, \end{cases} \qquad B^1(t) \triangleq \sum_{l \in \mathbb{Z}} \chi[-1/2, 1/2](t + Nl). \tag{2.3}$$

The Fourier coefficients of the B-spline

$$c_n(B^1) = \int_{-N/2}^{N/2} B^1(t)\, e^{-2\pi i n t/N} = \int_{-1/2}^{1/2} e^{-2\pi i n t/N} = \frac{\sin \pi n/N}{\pi n/N}.$$

The B-splines of higher order are defined iteratively via the circular convolution $B^p(t) \triangleq B^1 \circledast B^{p-1}(t)$. Thus, the B-spline $B^p(t)$ can be expanded into the Fourier series

$$B^p(t) = \frac{1}{N} \sum_{n \in \mathbb{Z}} e^{2\pi i n t/N} \left(\frac{\sin \pi n/N}{\pi n/N} \right)^p. \tag{2.4}$$

The B-spline $B^p(t)$ is supported on the interval $(-p/2, p/2)$ (up to periodization), it is strictly positive inside this interval and symmetric about zero, where it has its single maximum. The B-spline B^p consists of pieces of polynomials of degree $p-1$ that are linked to each other at the nodes such that $B^p \in C^{p-2}$. An explicit expression for the B-spline at the interval $(-N/2, N/2)$ is:

$$B^p(t) = \frac{1}{(p-1)!} \sum_{k=0}^{p} (-1)^p \binom{p}{k} \left(t + \frac{p}{2} - k \right)_+^{p-1}, \quad t_+ \triangleq \begin{cases} t, & \text{if } t \geq 0; \\ 0, & \text{otherwise.} \end{cases} \tag{2.5}$$

Surely, the length $p+1$ of the spline's B^p support should not exceed the period N, thus $p+1 < N$.

The shifts of the periodic B-spline $\{B^p(t-k)\},\ k = 0, ..., N-1,\ p \in \mathbb{N}$, form a basis for the space ${}^p\mathcal{S}$. Each spline $S^p(t) \in {}^p\mathcal{S}$ can be represented as

$$S^p(t) = \sum_{k=0}^{N-1} q[k] B^p(t-k), \quad \mathbf{q} = \{q[k]\} \in \Pi[N]. \tag{2.6}$$

The Fourier coefficients of the spline $S^p(t)$ are

$$\begin{array}{rcl} c_n(S^p) & = & \int_{-N/2}^{N/2} e^{-2\pi i n t/N} \sum_{k=0}^{N-1} q[k] B^p(t-k)\, dt \\ & = & \sum_{k=0}^{N-1} e^{-2\pi i n k/N} q[k] \int_{-N/2}^{N/2} e^{-2\pi i n t/N} B^p(t)\, dt = \hat{q}[n] \left(\frac{\sin \pi n/N}{\pi n/N} \right)^p. \end{array} \tag{2.7}$$

2.2.2 Exponential splines

The splines

$$\zeta^p[n](t) \triangleq \sum_{k=0}^{N-1} \omega^{kn}\, B^p\,(t-k)\,, \quad n=0,...,N-1, \tag{2.8}$$

which belong to ${}^p\mathcal{S}$, are called the periodic exponential splines. They are the so-called Zak transforms of the periodic B-splines [21, 7].

By the application of the inverse DFT (IDFT) to Eq. (2.8), B-splines is expressed by the exponential splines $B^p\,(t-k) = N^{-1}\sum_{n=0}^{N-1}\zeta^p[n](t)\,\omega^{-kn}$. Substitution of this relation into Eq. (2.6), provides the following splines representation:

$$S^p(t) = \frac{1}{N}\sum_{k=0}^{N-1} q[k] \sum_{n=0}^{N-1}\zeta^p[n](t)\,\omega^{-kn} = \frac{1}{N}\sum_{n=0}^{N-1}\sigma[n]\,\zeta^p[n](t), \quad \sigma[n] \triangleq \hat{q}[n]. \tag{2.9}$$

Representation in Eq. (2.9) of periodic splines by exponential splines generates a kind of harmonic analysis in the spline spaces that is called spline harmonic analysis (SHA) [22, 4, 6], where the splines $\zeta^p[n](t)$ are the counterparts of the Fourier exponentials. We describe a few properties of the exponential splines, which will be used later.

Proposition 2.1 *The following properties of the exponential splines $\zeta^p[n](t) \in {}^p\mathcal{S}$ hold:*

1. *Expansion into a Fourier series*

$$\zeta^p[n]\,(t) = \sum_{l\in\mathbb{Z}} e^{2\pi i(n/N+l)t}\,\left(\frac{\sin\pi\,(n/N+l)}{\pi\,(n/N+l)}\right)^p = \sin^p\frac{\pi n}{N}\sum_{l\in\mathbb{Z}} e^{2\pi i(n/N+l)t}\,\left(\frac{(-1)^l}{\pi\,(n/N+l)}\right)^p. \tag{2.10}$$

2. *The exponential splines $\zeta^p[n](t)$ are the eigenfunctions of the integer shift operator:*

$$\zeta^p[n]\,(t+d) = \omega^{nd}\zeta^p[n](t) \Longrightarrow \zeta^p[n]\,(d) = \omega^{nd}\,u^p[n],\ d\in\mathbb{Z}. \tag{2.11}$$

3. *The exponential splines $\zeta^p[n](t)$, $n=0,...N-1$, form an orthogonal basis for the space ${}^p\mathcal{S}$.*

Proof:

1. Equations (2.7) and (2.8) imply that the Fourier coefficients of $\zeta^p[n]$

$$c_\nu(\zeta^p[n]) = \sum_{k=0}^{N-1} e^{2\pi ik(n-\nu)/N}\,c_\nu(B^p) = N\,\delta[n-\nu](\mathrm{mod}N)\,\left(\frac{\sin\pi n/N}{\pi n/N}\right)^p. \tag{2.12}$$

   Hence, Eq. (2.10) follows.

2. Equation (2.11) is derived from the definition of the exponential splines in Eq. (2.8).

3. From the Parseval identity of periodic functions we have

$$\int_0^N \zeta^p[n]\,(t)\;\zeta^p[r]\,(t)^*\;dt = \frac{1}{N}\sum_{\nu\in\mathbb{Z}} c_\nu(\zeta^p[n])\,c_\nu^*(\zeta^p[r]) = N\,\delta(n-r]\sum_{l\in\mathbb{Z}}\left(\frac{\sin\pi\,(n/N+l)}{\pi\,(n/N+l)}\right)^{2p}. \quad (2.13)$$

Thus, the splines $\zeta^p[n]$ and $\zeta^p[r]$ are orthogonal to each other and the set $\{\zeta^p[n]\}, n = 0, ..., N-1$, forms an orthogonal basis of the space ${}^p\mathcal{S}$.

■

The N-periodic sequence

$$u^p[n] \triangleq \zeta^p[n](0) = \sum_{k=0}^{N-1} e^{-2\pi i n k/N} B^p\,(k) = \sum_{l\in\mathbb{Z}}\left(\frac{\sin\pi\,(n/N+l)}{\pi\,(n/N+l)}\right)^p = \sin^p\frac{\pi n}{N}\sum_{l\in\mathbb{Z}}\left(\frac{(-1)^l}{\pi\,(n/N+l)}\right)^p \quad (2.14)$$

is called the characteristic sequence of the space ${}^p\mathcal{S}$.

Remark 2.1 *By comparing Eq. (2.13) with Eq. (2.14), we observe that the squared norms of the exponential splines are* $\|\zeta^p[n]\|^2 = N\,u^{2p}[n]$.

Equation (2.14) implies that the characteristic sequence $u^p[n]$ is calculated by the DFT of the sampled B-splines. Table 2.1 provides samples of B-splines $B^p(t)$ of orders from 2 to 10 at grid points. The samples of higher order B-splines can be calculated by Eq. (2.5).

k	-4	-3	-2	-1	0	1	2	3	4
$B^2(k)$	0	0	0	0	1	0	0	0	0
$B^3(k)\times 8$	0	0	0	1	6	1	0	0	0
$B^4(k)\times 6$	0	0	0	1	4	1	0	0	0
$B^5(k)\times 384$	0	0	1	76	230	76	1	0	0
$B^6(k)\times 120$	0	0	1	26	66	26	1	0	0
$B^7(k)\times 2^6\,6!$	0	1	722	10543	23548	10543	722	1	0
$B^8(k)\times 7!$	0	1	120	1191	2416	1191	120	1	0
$B^9(k)\times 2^8\,7!$	1	6552	331610	2485288	4675014	2485288	331610	6552	1
$B^{10}(k)\times 9!$	1	502	14608	88234	156190	88234	14608	502	1

Table 2.1: Values of the B-splines B^p at grid points.

The B-splines are compactly supported and symmetric about zero. Therefore, the sequences $u^p[n]$ are cosine polynomials $u^p[n] = P_r(\cos\pi n/N)$ of degree $r = [(p+1)/2]$ with real coefficients, which only have even degree terms. They are strictly positive and symmetric about $N/2$.

Examples of characteristic sequences: Denote $y = \cos \pi n/N$. Then

$$u_2^p = 1, \quad u^3[n] = \frac{1+y^2}{2}, \quad u^4[n] = \frac{1+2y^2}{3}. \tag{2.15}$$

$$u^5[n] = \frac{5+18y^2+y^4}{24}, \quad u^6[n] = \frac{2+11y^2+2y^4}{15}, \tag{2.16}$$

$$u^7[n] = \frac{y^6+179y^4+479y^2+61}{720}, \; u^8[n] = \frac{16y^6+4740y^4-4635y^2+1139}{1260}. \tag{2.17}$$

Proposition 2.2 *The s-th ($s < p$) derivatives of the exponential splines $\zeta^p[n](t)$ are orthogonal to each other and their squared norms are*

$$\left\| (\zeta^p[n])^{(s)} \right\|^2 = N \left(2 \sin^2 \frac{\pi n}{N} \right)^{2s} u^{2(p-s)}[n]. \tag{2.18}$$

Proof: The derivative of the exponential splines $\zeta^p[n](t)$ is

$$\zeta^p[n]\,(t)^{(s)} = (2i)^s \, \sin^p \frac{\pi n}{N} \sum_{l \in \mathbb{Z}} e^{2\pi i (n/N+l)t} \left(\frac{(-1)^l}{\pi\,(n/N+l)} \right)^{p-s}.$$

The orthogonality of the derivatives of the different exponential splines $\zeta^p[n](t)$ is derived from the same reason that the orthogonality of the exponential splines. The squared norms are

$$\left\| (\zeta^p[n])^{(s)} \right\|^2 = N \left(2 \sin^2 \frac{\pi n}{N} \right)^{2s} \sin^{2(p-s)} \frac{\pi n}{N} \sum_{l \in \mathbb{Z}} \left(\frac{1}{\pi\,(n/N+l)} \right)^{2(p-s)} = N \left(2 \sin^2 \frac{\pi n}{N} \right)^{2s} u^{2(p-s)}[n].$$

■

Proposition 2.2 implies a Parseval identity type.

Corollary 2.1 *The squared norm of the s-th derivative of a spline $S(t) = N^{-1} \sum_{n=0}^{N-1} \sigma[n]\, \zeta^p[n](t) \in {}^p\mathcal{S}$ is*

$$\left\| (S^{(s)} \right\|^2 = \frac{1}{N} \sum_{n=0}^{N-1} \left(2 \sin \frac{\pi n}{N} \right)^{2s} u^{2(p-s)}[n]\, |\sigma[n]|^2. \tag{2.19}$$

2.3 Interpolation

A spline, which interpolates a periodic signal $\mathbf{x}$, can be explicitly represented in the basis of exponential splines.

Proposition 2.3 *Any N-periodic signal $\boldsymbol{x} = \{x[k]\}$, $k \in \mathbb{Z}$, can be uniquely interpolated by a spline $S(k) = x[k]$ from ${}^p\mathcal{S}$.*

Proof: Assume a spline $S^p \in {}^p\mathcal{S}$ is expanded over the basis of the exponential splines: $S^p(t) = N^{-1} \sum_{n=0}^{N-1} \sigma[n]\, \zeta^p[n](t)$. Then, its grid samples are

$$S^p(k) = \frac{1}{N} \sum_{n=0}^{N-1} \sigma[n]\, \zeta^p[n](k) = \frac{1}{N} \sum_{n=0}^{N-1} \sigma[n]\, \omega^{kn}\, \zeta^p[n](0) = \frac{1}{N} \sum_{n=0}^{N-1} \sigma[n]\, \omega^{kn}\, u^p[n]. \tag{2.20}$$

By the application of the DFT to both sides of the equation $S^p(k) = \frac{1}{N} \sum_{n=0}^{N-1} \sigma[n]\, \omega^{kn}\, u^p[n] = x[k]$ we get $\sigma[n]\, u^p[n] = \hat{x}[n]$. Since $u^p[n] > 0$, we derive an explicit expression for the interpolating spline

$$S^p(t) = \frac{1}{N} \sum_{n=0}^{N-1} \frac{\hat{x}[n]}{u^p[n]}\, \zeta^p[n](t). \tag{2.21}$$

■

2.3.1 Minimal norm property of even order splines

Splines of even orders from the spaces ${}^{2r}\mathcal{S}$ possess a remarkable property. Assume $\mathbf{x} = \{x[k]\}$ is an N-periodic signal and denote by $\mathcal{F}_x^r$ the space of N-periodic functions $f(t)$ such that the functional $I(f) \triangleq \int_0^N (f^{(r)}(t))^2\, dt < \infty$ and $f(k) = x[k],\ k \in \mathbb{Z}$.

Proposition 2.4 ([10, 2]) *The spline $S^{2r}(t) \in {}^{2r}\mathcal{S}$ of even order $2r$, which interpolates the signal $\mathbf{x}$, yields the minimum to the functional $I(f)$ on the space $\mathcal{F}_x^r$:*

$$S^{2r}(t) = \arg \min_{f \in \mathcal{F}_x^r} \int_0^N (f^{(r)}(t))^2\, dt. \tag{2.22}$$

In particular, the cubic interpolatory spline $S^4(t)$ minimizes the "energy" integral

$$S^4(t) = \arg \min_{f \in \mathcal{F}_x^2} \int_0^N (f''(t))^2\, dt. \tag{2.23}$$

The claim of the proposition remains true even when the signals samples are defined on a non-uniform grid. The integral in Eq. (2.23) is related to the curvature, therefore the cubic spline's plot describes a minimum curvature line, which passes through a given set of points on the plane. To draw such lines, draftsmen used splines – flexible wood or metal strips. Splines owe their names for that.

2.3.2 Fundamental splines

Equation (2.21) is, in a way, similar to the Fourier expansion of the interpolating spline $S^p(t)$. There exists an explicit time domain representation of a spline. It is readily derived from Eq. (2.21). Using the shift property Eq. (2.11) of the exponential splines, we have

$$S^p(t) = \frac{1}{N} \sum_{n=0}^{N-1} \frac{\zeta^p[n](t)}{u^p[n]} \sum_{k=0}^{N-1} \omega^{-nk}\, x[k] = \frac{1}{N} \sum_{k=0}^{N-1} x[k] \sum_{n=0}^{N-1} \frac{\zeta^p[n](t-k)}{u^p[n]}$$

$$\Longrightarrow S^p(t) = \sum_{k=0}^{N-1} x[k]\, \varphi^p(t-k), \quad \varphi^p(t) \triangleq \frac{1}{N} \sum_{n=0}^{N-1} \frac{1}{u^p[n]}\, \zeta^p[n](t). \tag{2.24}$$

The function $\varphi^p(t)$ is represented via the exponential splines basis as in Eq. (2.9) with the coefficients $\sigma[n] = 1/u^p[n]$. Therefore, $\varphi^p(t)$ is a spline from ${}^p\mathcal{S}$. It is called the fundamental spline of the space ${}^p\mathcal{S}$. The coefficients $\sigma[n]$ are the DFT of the B-spline coefficients. Thus, the spline $\varphi^p(t)$ can be represented as $\varphi^p(t) = \sum_{k=0}^{N-1} f[k]\, B^p(t-k)$ where the coefficients $f[k] = N^{-1} \sum_{n=0}^{N-1} \omega^{kn}/u^p[n]$. Equation (2.20) implies that the grid values of the fundamental spline are

$$\varphi^p(k) = \frac{1}{N} \sum_{n=0}^{N-1} \omega^{kn} \frac{u^p[n]}{u^p[n]} = \frac{1}{N} \sum_{n=0}^{N-1} \omega^{kn} = \delta[k](\mathrm{mod} N).$$

This property is similar to the property of the *sinc* function $\mathrm{sinc}(t) \triangleq \sin \pi t/\pi t$. The *sinc* function represents bandlimited functions via their samples ([16], for example): If the Fourier spectrum of a non-periodic signal $f(t)$ is located within the band $[-\sigma, \sigma]$, then it can be represented as $f(t) = \sum_{k\in\mathbb{Z}} f(Pk)\,\mathrm{sinc}(\sigma\,(t-Pk))$, where $P = \pi/\sigma$.

The Fourier transform of the *sinc* function is $C(v) \triangleq \int_{-\infty}^{\infty} e^{-ivt}\,\mathrm{sinc}(t)\,dt = \chi[-\pi,\pi](v)$, where the function χ is defined in Eq. (2.3). Denote by $\mathrm{Sinc}_N(t) \triangleq \sum_{l\in\mathbb{Z}} \mathrm{sinc}\,(t+lN)$ the periodized *sinc* function. The Fourier coefficients of the periodic function $\mathrm{Sinc}_N(t)$ are

$$c_n\left(\mathrm{Sinc}_N\right) = C\left(\frac{2\pi n}{N}\right) = \begin{cases} 1, & \text{if } |n| \le N/2; \\ 0, & \text{otherwise} \end{cases} \Longrightarrow \mathrm{Sinc}_N(t) = \frac{1}{N} \sum_{n=-N/2}^{N/2} e^{2\pi i n t/N} = \frac{\sin \pi t(1+1/N)}{N\,\sin \pi t/N}.$$

Apparently, $\mathrm{Sinc}_N(t) \to \mathrm{sinc}(t)$ as the period $N \to \infty$.

The Fourier spectra of the fundamental splines $\varphi^p(t)$ approach the Fourier spectrum of the *sinc* function when the splines orders increase. Such a convergence is established in [3] for the non-periodic fundamental splines. The statement for the periodic case is the following.

Theorem 2.1 *All the Fourier coefficients $c_n(\varphi^p)$, where $|n| < N/2$, of the $N-$periodic fundamental splines tend to 1 when the spline order p is growing. The coefficients, whose indices $n > N/2$ or $n < -N/2$ tend to zero as p is growing. The coefficients $c_{\pm N/2}(\varphi^p)$ tend to 1/2 as p is growing.*

Proof: We prove the statement for the even order splines $\varphi^{2r}(t)$. Proof for the odd order splines differs in a few non-essential details. Equations (2.7) and (2.14) imply that the Fourier coefficients are

$$\begin{aligned} & c_n(\varphi^{2r}) = \frac{1}{u^{2r}[n]} \left(\frac{\sin \pi n/N}{\pi n/N}\right)^{2r} = \frac{1}{D^{2r}[n]}, \\ & D^{2r}[n] \triangleq \left(\frac{\pi n}{N}\right)^{2r} \sum_{l\in\mathbb{Z}} \frac{1}{\left(\pi\,(n/N+l)\right)^{2r}} = \sum_{l\in\mathbb{Z}} \frac{1}{\left(1+N\,l/n)\right)^{2r}} \\ & = 1 + \sigma[n,2r], \quad \sigma[n,2r] \triangleq \sigma_+[n,2r] + \sigma_-[n,2r], \quad \sigma_\pm[n,2r] \triangleq \sum_{l=1}^{\infty} \frac{1}{\left(1\pm N\,l/n)\right)^{2r}}. \end{aligned}$$

Note that the coefficients $c_{lN} = 0$ for all the integers $l \neq 0$, while $c_0 = 1$ and all the coefficients are non-negative and do not exceed 1. The series $\sigma_\pm[n,2r]$ converge with any integer $n \neq kN$. Assume that

$0 < n < N/2$. The terms in the series $\sigma_+[n,l,2r]$ decrease monotonically as l grows. Therefore, its sum becomes

$$|\sigma_+[n,2r]| < \frac{1}{\left(1+N/n)\right)^{2r}} + \int_1^\infty \frac{1}{(1+Nt/n)^{2r}}\,dt < \alpha_+[2r], \quad \alpha_+[2r] \triangleq \frac{1}{3^{2r}} + \frac{2r+1}{2^{2r+2}}.$$

The sum of the series $\sigma_-[n,l,2r]$ is

$$\sigma_-[n,2r]| < \frac{1}{\left(1-N/n)\right)^{2r}} + \frac{1}{\left(1-2N/n)\right)^{2r}} + \int_2^\infty \frac{1}{(1-Nt/n)^{2r}}\,dt < \alpha_-[n,2r],$$
$$\alpha_-[n,2r] \triangleq \left(\frac{N-n}{n}\right)^{2r} + \alpha_+[2r].$$

Consequently,

$$c_n(\varphi^{2r}) = \frac{1}{1+\sigma[n,2r]} = 1 - \sigma[n,2r] + \sum_{l=2}^{\infty}(-\sigma[n,2r])^l = 1 - \beta[n,2r],$$
$$0 < \beta[n,2r] < \sigma[n,2r] < \left(\frac{N-n}{n}\right)^{2r} + 2\,\alpha_+[2r].$$

Thus, each coefficient $c_n(\varphi^{2r})$, $0 \le n < N/2$, is approaching 1 as the spline order $2r$ increases. Recall that the order $2r$ cannot exceed $N-1$. The convergence speed is different for different n. When n is approaching $N/2$ then the convergence speed is decreasing. Obviously, the same claim is true for $-N/2 < n < 0$.

If $n > N/2$ then $1 - N/n < 1$. Thus, the first term in the series $\sigma_-[n,2r]|$, which is $(1-N/n)^{-2r}$, grows when $2r$ increases while the sum of the remainder of the series is reduced as well as the series $\sigma_+[n,2r]|$. As a result, the coefficient $c_n(\varphi^{2r}) = 1/D^{2r}[n] = O\left((1-N/n)^{2r}\right)$. When $n > N/2$ is growing then the coefficients are converging fast to 0.

Let $n = N/2$. Then,

$$\sigma_+[n,2r] = \sum_{l=1}^{\infty} \frac{1}{\left(1+2l)\right)^{2r}} < \frac{1}{2^{2r}}\,C_+, \quad C_+ \triangleq \sum_{l=1}^{\infty} \frac{1}{l^{2r}},$$
$$\sigma_-[n,2r] = 1 + \beta_-[2r], \quad \beta_-[2r] \triangleq \sum_{l=2}^{\infty} \frac{1}{\left(1-2l)\right)^{2r}} < \frac{1}{2^{2r}}\,C_-, \quad C_- \triangleq \sum_{l=2}^{\infty} \frac{1}{l^{2r}}.$$

Thus, $D^{2r}[\pm N/2] = 2 + O(2^{-2r})$. ■

Corollary 2.2 *The fundamental splines $\varphi^p(t)$ are approaching the periodic sinc function* $\mathrm{Sinc}(t)$ *as the spline orders p are increasing.*

Figure 2.1 displays the fundamental splines $\varphi^p(t)$ of orders 2, 6, 10, 14 and their Fourier coefficients. We observe that the effective supports of the splines widen and their behavior becomes oscillating as the orders increase, while the shapes of their spectra tend to the rectangle.

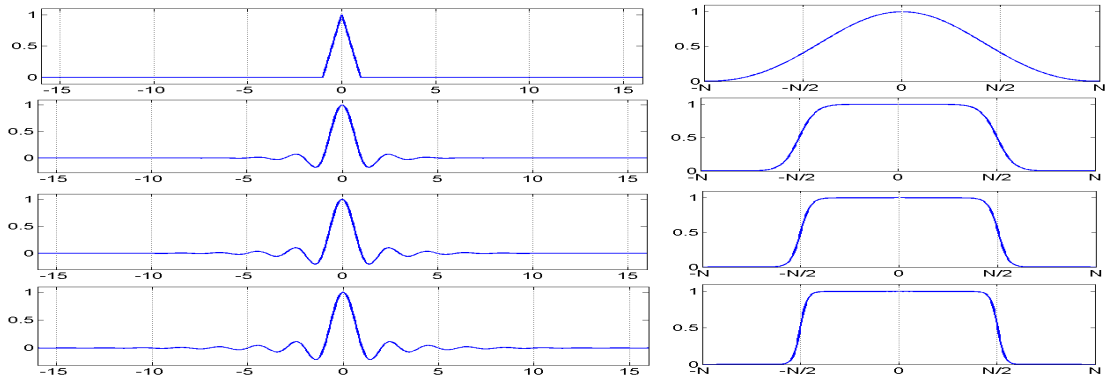

Figure 2.1: Left: fundamental splines $\varphi^{2r}(t)$ of orders (from top to bottom) 2, 6, 10, 14. Right: their Fourier coefficients

Figure 2.2 compares the fundamental spline $\varphi^{22}(t)$ of order 22 with the periodic *sinc* function $\mathrm{Sinc}_N(t)$, $N = 512$. When t is not far from zero (up to 5), the two functions are almost undistinguishable. When t grows, the spline practically vanishes while $\mathrm{Sinc}_N(t)$ oscillates. The spectrum of the spline is near a perfect rectangle.

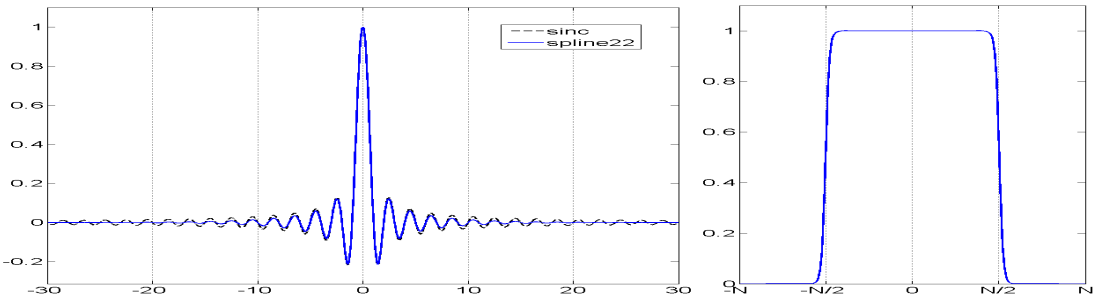

Figure 2.2: Left: fundamental splines $\varphi^{22}(t)$ of order 22 (solid line) and *sinc* function $\mathrm{Sinc}_N(t)$, $N = 512$ (dashed line). Right: the Fourier coefficients of this spline

2.4 Smoothing splines

When the samples of a signal $f(t)$ are known up to some errors, it does not make sense to interpolate these samples because it will result in an irregular function, which hardly fits the signal $f(t)$, especially if $f(t)$ is smooth. A natural idea, which can be traced to Whittaker paper [19] from 1923, is to relax the interpolation requirement while introducing a smoothness constraint. This approach was formalized by Schoenberg [14] in 1964. In the periodic case, usage of the SHA enables to explicitly construct the solution in one and several -dimensions by smoothing splines. We briefly outline the design scheme.

2.4.1 One-dimensional smoothing splines

Denote by $\mathcal{F}^r$ the subspace of the continuous-time $N-$periodic signals $\varphi(t)$ such that the functional $I(\varphi) \triangleq \int_0^T (\varphi^{(r)}(t))^2\, dt < \infty$. Assume that the signal to be approximated is $f(t) \in \mathcal{F}^r$, $\mathbf{y} = \{y[k] = f(k) + e_k\}$, $k = 0, ..., N-1$, where $\mathbf{e} = \{e_k\}$ is the vector of random errors, which is a zero-mean white noise. In addition, assume that the sum $\varepsilon^2 \triangleq \sum_{k=0}^{N-1} e_k^2$ can be evaluated.

The signal $f(t)$ is approximated by a function $g(t) \in \mathcal{F}^r$, which yields the minimum to the functional I subject to the condition that the discrepancy functional $E_y(g) \triangleq \sum_{k=0}^{N-1} |g(k) - y[k]|^2 \le \varepsilon^2$.

This constrained minimization problem is reduced to the solution of an unconstrained problem: $g_\rho(t) = \arg\min_{g\in\mathcal{F}^r} (J_\rho(g))$, $J_\rho(g) \triangleq \rho\, I(g) + E(g)$ followed by derivation of the numerical parameter ρ from the equation $e(\rho) \triangleq E_y(g_\rho) = \varepsilon^2$.

Proposition 2.5 ([14]) *A unique solution to the minimization problem* $\min_{g\in\mathcal{F}^r} J_\rho(g)$ *is a spline* $S_\rho[\mathbf{y}](t) \in {}^{2r}\mathcal{S}$ *of even order* $2r$.

The spline $S_\rho(t) \in {}^{2r}\mathcal{S}$, which minimizes the functional J_ρ, is called the periodic smoothing spline. The spline $S_\rho(t)$ can be explicitly expressed via the exponential splines basis. Assume a spline is represented as $S(t) = N^{-1} \sum_{n=0}^{N-1} \sigma[n]\, \zeta^{2r}[n](t)$. Equation (2.19) implies that the functional

$$I(S) = \frac{1}{N} \sum_{n=0}^{N-1} \left(2 \sin \frac{\pi n}{N}\right)^{2r} u^{2r}[n]\, |\sigma[n]|^2. \tag{2.25}$$

Due to Eq. (2.20), the grid samples of $S(t)$ are $S(k) = N^{-1} \sum_{n=0}^{N-1} \sigma[n]\, \omega^{kn}\, u^{2r}[n]$. Thus, the functional

$$E_y(S) = \frac{1}{N} \sum_{n=0}^{N-1} \left|\sigma[n]\, u^{2r}[n] - \hat{y}[n]\right|^{2r}, \quad \hat{y}[n] = \sum_{k=0}^{N-1} \omega^{-kn}\, y[k]. \tag{2.26}$$

An explicit solution to the unconstrained minimization problem is derived from using Eqs. (2.25) and (2.26). It is the spline from ${}^{2r}\mathcal{S}$

$$S_\rho^{2r}(t) = \frac{1}{\sqrt{N}} \sum_{n=0}^{N-1} \sigma[n](\rho)\, \zeta^{2r}[n](t), \quad \sigma[n](\rho) = \frac{\hat{y}[n]}{\rho\, (2 \sin \pi n/N)^{2r} + u^{2r}[n]}. \tag{2.27}$$

The discrepancy functional for the parameterized spline $S_\rho^{2r}(t)$

$$e(\rho) \triangleq E_y(S_\rho) = \frac{1}{N} \sum_{n=0}^{N-1} \left|\sigma[n](\rho)\, u^{2r}[n] - \hat{y}[n]\right|^{2r} = \frac{1}{N} \sum_{n=0}^{N-1} |\hat{y}[n]|^2 \left(\frac{\rho\, (2 \sin \pi n/N)^{2r}}{\rho\, (2 \sin \pi n/N)^{2r} + u^{2r}[n]}\right)^2. \tag{2.28}$$

In order to derive an optimal value for the parameter ρ, we have to solve the equation $e(\rho) = \varepsilon^2$. The function $e(\rho)$ grows monotonically from $e(0) = 0$ to $e(\infty) = N^{-1} \sum_{n=0}^{N-1} |\hat{y}[n]|^2 = \|\mathbf{y}\|^2$. Therefore, the equation has a unique solution $\rho = \bar{\rho}$. The spline $S_{\bar{\rho}}^{2r}(t)$ solves the constrained minimization problem. Its grid samples are

$$S_{\bar{\rho}}^{2r}(k) = \frac{1}{N} \sum_{n=0}^{N-1} \sigma[n](\bar{\rho})\, \omega^{kn}\, u^{2r}[n] = \frac{1}{N} \sum_{n=0}^{N-1} \omega^{kn}\, \frac{\hat{y}[n]\, u^{2r}[n]}{\bar{\rho}\, (2 \sin \pi n/N)^{2r} + u^{2r}[n]}. \tag{2.29}$$

The samples are readily calculated by the IDFT.

Remark 2.2 *The spline $S^{2r}_{\bar\rho}(t)$ can be regarded as a spline that interpolates the signal $\mathbf{s} = \left\{S^{2r}_{\bar\rho}(k)\right\}$. The values between grid points are calculated by the subdivision methods that are described in Sections 3 and 4.*

When the errors do not present, that is $\varepsilon = 0$, then the parameter is $\bar\rho = 0$ and the grid samples are $S^{2r}_{\bar 0}(k) = y[k] = f(k)$. Thus, the smoothing spline reduces to an interpolating spline.

2.4.2 Two-dimensional splines

The two-dimensional N-periodic function $S(x,y) \triangleq \sum_{k,n=0}^{N-1} s[k,n]\, B^p(x-k)\, B^q(y-n)$ is a 1D spline of order p with respect to x when the variable y is fixed and a 1D spline of order q with respect to y when the fixed variable is x. It is called the 2D spline on the grid $\{k,n\}$, $k,n \in \mathbb{Z}$, and the space of such splines is denoted as ${}^{p,q}\mathcal{S}$. An alternative representation of the splines is provided by the exponential splines $S(x,y) = N^{-2}\sum_{\kappa,\nu=0}^{N-1} \sigma[\kappa,\nu]\, \zeta^p[\kappa](x)\, \zeta^q[\nu](y)$. The grid samples of the spline S are

$$S(k,n) = \frac{1}{N^2}\sum_{\kappa,\nu=0}^{N-1} e^{2\pi i(k\kappa+n\nu)}\sigma[\kappa,\nu]\, u^p[\kappa]\, u^q[\nu]. \tag{2.30}$$

Consequently, the spline $S(x,y) \in {}^{p,q}\mathcal{S}$, which interpolates an N-periodic signal $\mathbf{z} \triangleq \{z[k,n]\}$, that is $S(k,n) = z[k,n]$, is explicitly represented as

$$S(x,y) = \frac{1}{N^2}\sum_{\kappa,\nu=0}^{N-1} e^{2\pi i(k\kappa+n\nu)}\frac{\hat z[\kappa,\nu]}{u^p[\kappa]\, u^q[\nu]}, \quad \hat z[\kappa,\nu] \triangleq \sum_{k,n=0}^{N-1} e^{-2\pi i(k\kappa+n\nu)} z[k,n]. \tag{2.31}$$

The design of the two-dimensional smoothing splines is implemented by the same steps as in the 1D design. For simplicity, assume that the splines have the same order in both x and y directions. Assume that an N-periodicin both directions function $\varphi(x,y)$ is approximated such that the functional satisfies

$$I(\varphi) \triangleq \int_0^N \left((\varphi^{(r)}_x(x,y))^2 + (\varphi^{(r)}_y(x,y))^2\right) dx\, dy < \infty.$$

Assume that $\mathbf{z} = \{z[k,n] = f(k,n) + e_{k,n}\}$, $k,n = 0,...,N-1$, $\mathbf{e} = \{e_{k,n}\}$, $k,n = 0,...,N-1$, is the array of random errors that is assumed to be a zero-mean white noise. The estimated squared norm of errors is $\varepsilon^2 = \sum_{k,n=0}^{N-1} e^2_{k,n}$. Denote by $S_\rho(x,y) \in {}^{2r,2r}\mathcal{S}$ the spline, which minimizes the parameterized functional $J_\rho(S) \triangleq \rho I(S) + E_z(S)$ on the space ${}^{2r,2r}\mathcal{S}$. The discrepancy functional $E_z(S)$ is defined as $E_z(S) \triangleq \sum_{k,n=0}^{N-1}(S(k,n) - z[k,n])^2$. Equation (2.30) implies that

$$E_z(S) = \frac{1}{N^2}\sum_{\kappa,\nu=0}^{N-1}\left|\sigma[\kappa,\nu]\, u^{2r}[\kappa]\, u^{2r}[\nu] - \hat z[\kappa,\nu]\right|^2. \tag{2.32}$$

The functional

$$I(S) = \frac{1}{N^2}\sum_{\kappa,\nu=0}^{N-1}\left(W^r[\kappa,\nu] + W^r[\nu,\kappa]\right)|\sigma[\kappa,\nu]|^2, \quad W^r[\kappa,\nu] \triangleq \left(2\sin\frac{\pi n}{N}\right)^{2r} u^{2r}[\kappa]\, u^{4r}[\nu]. \tag{2.33}$$

By using Eqs. (2.32) and (2.33), the spline is explicitly represented as

$$S_\rho(x,y) = \frac{1}{N^2}\sum_{\kappa,\nu=0}^{N-1} \sigma[\kappa,\nu](\rho)\,\zeta^{2r}[\kappa](x)\,\zeta^{2r}[\nu](y), \quad \sigma[\kappa,\nu](\rho) \triangleq \frac{\hat{z}[\kappa,\nu]\,u^{2r}[\kappa]\,u^{2r}[\nu]}{A^r[\kappa,\nu](\rho)}, \tag{2.34}$$

$$A^r[\kappa,\nu](\rho) \triangleq \rho\,(W^r[\kappa,\nu] + W^r[\nu,\kappa]) + (u^{2r}[\kappa]\,u^{2r}[\nu])^2.$$

Similar to the 1D case, an optimal regularization parameter ρ is derived from the equation $e(\rho) \triangleq E_z(S_\rho) = \varepsilon^2$, which is expressed as

$$e(\rho) = \frac{1}{N^2}\sum_{\kappa,\nu=0}^{N-1} |\hat{z}[\kappa,\nu]|^2 \left(\frac{(\rho\ (W^r[\kappa,\nu] + W^r[\nu,\kappa])}{A^r[\kappa,\nu](\rho)}\right)^2 = \varepsilon^2, \tag{2.35}$$

which has a unique solution $\rho = \bar{\rho}$. The grid values of the spline $S_{\bar{\rho}}(x,y)$, which is called the 2D smoothing spline, are

$$S_{\bar{\rho}}(k,n) = \frac{1}{N^2}\sum_{\kappa,\nu=0}^{N-1} e^{2\pi i(k\kappa+n\nu)}\frac{\hat{z}[\kappa,\nu]\,(u^{2r}[\kappa]\,u^{2r}[\nu])^2}{\bar{\rho}\,(W^r[\kappa,\nu] + W^r[\nu,\kappa]) + (u^{2r}[\kappa]\,u^{2r}[\nu])^2}. \tag{2.36}$$

The grid values are calculated by the 2D IDFT. Certainly, when $\varepsilon^2 = 0$, the parameter $\bar{\rho} = 0$ and the spline $S_{\bar{\rho}}(x,y)$ interpolates the initial function $f(x,y)$ such that $S_0(k,n) = f(k,n)$.

3 Dyadic subdivision for periodic splines

In this section, we present explicit formulas for calculation of values of a spline $S^{2r}(t) \in {}^{2r}\mathcal{S}$ of even order $2r$ at dyadic rational points $\{k/2^m\},\ k \in \mathbb{Z},\ m \in \mathbb{N}$, under the assumption that its samples on the grid $\mathbf{g} = \{k\},\ k \in \mathbb{Z}$, are available: $S(k) = y[k]$. In this case, utilization of the exponential splines makes the splines computations of arbitrary even orders straightforward.

3.1 Spline spaces of different dyadic resolution scales

So far, we used splines from the spaces ${}^p\mathcal{S}$, whose nodes are located on the grid $\{k\}$. In this section, we introduce an embedded set of periodic splines spaces that correspond to different dyadic resolution scales.

As in previous sections, $N = 2^j,\ N_m = 2^m N = 2^{j+m},\ j,m \in \mathbb{N}$ and $\omega \triangleq e^{2\pi i/N}$. Denote by ${}^p\mathcal{S}_m$ the space of $N-$periodic splines of order p on the grid $\{k/2^m\}$. We retain the notation ${}^p\mathcal{S}$ for the space ${}^p\mathcal{S}_0$. Obviously, the space ${}^p\mathcal{S}_m$ is a subspace of ${}^p\mathcal{S}_{m+1}$. Thus, we get a set of periodic splines spaces that correspond to different resolution scales such that ${}^p\mathcal{S} \subset {}^p\mathcal{S}_1 .... \subset {}^p\mathcal{S}_m ...$.

The function $\beta_m^1(t)$ is defined to be zero outside the interval $(-2^{-m-1}, 2^{-m-1})$ and it is equal to 2^m inside the interval. The N-periodic normalized B-spline of the first order on the grid $\{2^{-m}\,k\}$ and its Fourier coefficients are

$$B_m^1(t) \triangleq \sum_{k\in\mathbb{Z}} \beta_m^1\,(t + kN)\,, \quad c_n(B_m^1) = \frac{\sin \pi n/N_m}{\pi n/N_m}.$$

The N-periodic normalized B-spline of order p is defined via the iterated circular convolution

$$B_m^p(t) \triangleq B_m^1 \circledast B_m^{p-1}(t) = \frac{1}{N} \sum_{n\in\mathbb{Z}} \left(\frac{\sin(\pi n/N_m)}{\pi n/N_m} \right)^p e^{2\pi i n t/N}. \tag{3.1}$$

Each spline $S_m(t) \in {}^p\mathcal{S}_m$ is represented by

$$S_m(t) = \sum_{k=0}^{N_m-1} q[k]\, B_m^p\left(t - 2^{-m}k\right) = \frac{1}{N_m} \sum_{n=0}^{N_m-1} \xi[n]\, \zeta_m^p[n](t), \quad \xi[n] = \hat{q}[n]_m, \tag{3.2}$$

where the exponential splines, which form orthogonal bases of ${}^p\mathcal{S}_m$, are the Zak transforms of the B-splines:

$$\zeta_m^p[n](t) \triangleq \sum_{k=0}^{N_m-1} \omega^{2^{-m}nk} B_m^p(t - 2^{-m}k) = 2^m \sum_{l\in\mathbb{Z}} e^{2\pi i(n/N + 2^m l)t} \left(\frac{\sin \pi(n/N_m + l)}{\pi(n/N_m + l)} \right)^p, \tag{3.3}$$

where $n = 0, ..., N_m - 1$. The N_m-periodic characteristic sequence of the space ${}^p\mathcal{S}_m$ is

$$u_m^p[n] \triangleq \zeta_m^p[n](0) = \sum_{k=0}^{N_m-1} \omega^{-2^{-m}nk} B_m^p(2^{-m}k) = 2^m \sum_{l\in\mathbb{Z}} \left(\frac{\sin \pi(n/N_m + l)}{\pi(n/N_m + l)} \right)^p. \tag{3.4}$$

The spline $S_m(t) \in {}^p\mathcal{S}_m$, which interpolates an N_m-periodic signal $\mathbf{x} = \{x[k]\}$ by $S(2^{-m}\, k) = x[k],\ k \in \mathbb{Z}$, is

$$S_m(t) = \frac{1}{N_m} \sum_{n=0}^{N_m-1} \frac{\hat{x}[n]_m}{u_m^p[n]}\, \zeta_m^p[n](t), \quad \hat{x}[n]_m = \sum_{k=0}^{N_m-1} \omega^{-2^{-m}nk} x[k]. \tag{3.5}$$

Proposition 3.1 *The characteristic sequence $u_m^p[n]$ of the space ${}^p\mathcal{S}_m$ can be calculated via the $2^m N-$point DFT of the sampled B-spline $B^p(t) \in {}^p\mathcal{S}$.*

Proof: Replace in Eq. (2.14) N to $N_m = 2^m N$ and compare the result with Eq. (3.4). Then, we get

$$\sum_{k=0}^{N_m-1} e^{-2\pi i n k/N_m} B^p(k) = \sum_{l\in\mathbb{Z}} \left(\frac{\sin \pi\,(n/N_m + l)}{\pi\,(n/N_m + l)} \right)^p = 2^{-m}\, u_m^p[n].$$

Thus, the sequence $u_m^p[n]$ is the $2^m N-$point DFT of the sampled B-spline $\left\{ b^p[k] \triangleq B^p(k) \right\}$ multiplied by 2^m to become

$$u_m^p[n] = 2^m\, \hat{b}^p[n]_m = 2^m \sum_{k=0}^{N_m-1} \omega^{-2^m kn} B^p(k). \tag{3.6}$$

■

Remark 3.1 *We retain the previous notations $\zeta^p[n](t) \equiv \zeta_0^p[n](t)$, $u^p[n] \equiv u_0^p[n]$ for splines on the initial scale ($m = 0$).*

3.2 Insertion rule

Calculation splines values of even order at dyadic rational points is implemented via the following refinement steps:

Dyadic periodic spline insertion rule: *Assume a spline $S_0(t)$ belongs to the space ${}^p\mathcal{S}$ and the samples $\mathbf{f}^0 \triangleq \left\{f^0[k] = S_0(k)\right\}$, $k \in \mathbb{Z}$ are available. For $m = 1, 2, \ldots$, we construct a spline $S_{m-1}(t) \in {}^p\mathcal{S}_{m-1}$ on the grid $\mathbf{g}^{m-1} \triangleq \left\{k/2^{m-1}\right\}$, , $k \in \mathbb{Z}$, which interpolates the sequence $\mathbf{f}^{m-1} \triangleq \left\{f^{m-1}[k]\right\}$: $S_{m-1}\left(k/2^{m-1}\right) = f^{m-1}[k]$, $k \in \mathbb{Z}$. Then, $f^m[k] \triangleq S_{m-1}\left(k/2^m\right)$, $k \in \mathbb{Z}$.*

In other words, in order to refine the data $\mathbf{f}^{m-1}$ from the grid $\left\{k/2^{m-1}\right\}$ to the grid $\{k/2^m\}$, we construct the spline $S_{m-1}(t)$, which interpolates $\mathbf{f}^{m-1}$ on the grid $\left\{k\,2^{m-1}\right\}$ and define $f^m[2k] \triangleq f^{m-1}[k]$, $\quad f^m[2k+1] \triangleq S_{m-1}((k+1/2)\,2^{m-1})$, that are the spline values at midpoints between the interpolation points.

If the order of the splines $S_m(t) \in {}^{2r}\mathcal{S}_m$ is even, then this insertion rule reproduces the spline, which means that $S_m(t) \equiv S_{m-1}(t) \equiv \ldots \equiv S_0(t)$. Consequently, each refinement step provides the spline $S_0(t)$ values at the subsequent set of dyadic rational points.

Theorem 3.1 *Let $S(t) \in {}^{2r}\mathcal{S}$ be an N-periodic spline of order $2r$ with nodes on the grid $\{k\}$, $k \in \mathbb{Z}$, and its samples are $\left\{S(k) = f^0[k]\right\}$, $\mathbf{f}^0 \triangleq \left\{f^0[k]\right\}$, $k \in \mathbb{Z}$. Then, all the subsequent subdivision steps with the dyadic spline insertion rule reproduce the values $\left\{f^m[k] = S(k/2^m)\right\}$, $k \in \mathbb{Z}$, $m = 1, 2, \ldots$ of this spline.*

Proof: Due to the minimal norm property (Proposition 2.4), we get

$$\mu \triangleq \int_0^N |S^{(r)}(t)|^2\,dt \le \int_0^N |g^{(r)}(t)|^2\,dt,$$

where $g(t)$ is any function such that $g^{(r)}(t)$ is square integrable and $\left\{g(k) = f^0[k]\right\}$, $k \in \mathbb{Z}$. Let $S_1(t) \in {}^{2r}\mathcal{S}_1$ be a spline of order $2r$, which interpolates the values $\{f^1[k] = S_1(k/2)\}_{k\in\mathbb{Z}}$. Then,

$$\nu \triangleq \int_0^N |S_1^{(r)}(t)|^2\,dt \le \int_0^N |G^{(r)}(t)|^2\,dt,$$

where $G(t)$ is any function such that $G^{(r)}(t)$ is square integrable and $G(k/2) = f^1[k] = S(k/2)$. Hence, $\nu \le \mu$. On the other hand, $S_1(k) = f^0[k]$, therefore, $\mu \le \nu$. Thus $\int_0^N |S^{(r)}(t)|^2\,dt = \int_0^N |S_1^{(r)}(t)|^2\,dt$. Hence, it follows that $S_1(t) \equiv S(t)$. Repeating the above reasoning, we find that the spline $S_2(t) \in {}^{2r}\mathcal{S}_2$, which interpolates the values $\{f^2[k] = S_1(k/4)\}_{k\in\mathbb{Z}}$, coincides with $S_1(t)$. Consequently, it coincides with $S(t)$. The same is true for any spline $S_m(t) \in {}^{2r}\mathcal{S}_{2^m}$, which interpolates the values $\{f^m[k] = S_{m-1}(k/2^m)\}_{k\in\mathbb{Z}}$. ■

3.3 Periodic spline filters for dyadic subdivision

The spline $S_0(t) \in {}^p\mathcal{S}$, which interpolates an N-periodic sequence $\mathbf{f}^0 \triangleq \left\{f^0[k]\right\}$ such that $S(k) = f^0[k]$, $k \in \mathbb{Z}$, is represented by

$$S_0(t) = \frac{1}{N}\sum_{n=0}^{N-1} \frac{\hat{f}^0[n]}{u^p[n]}\,\zeta^p[n](t), \quad \hat{f}^0[n] = \sum_{k\in\mathbb{Z}} \omega^{-kn} f^0[k], \tag{3.7}$$

$$\zeta^p[n](t) = \sum_{l\in\mathbb{Z}} e^{2\pi i(n/N+l)t} \left(\frac{\sin\pi\,(n/N+l)}{\pi\,(n/N+l)}\right)^p, \quad u^p[n] = \zeta^p[n](0) = \sum_{l\in\mathbb{Z}} \left(\frac{\sin\pi\,(n/N+l)}{\pi\,(n/N+l)}\right)^p. \tag{3.8}$$

The DFT of the refined array can be split into the polyphase components

$$\hat{f}^1[n]_1 = \sum_{k=0}^{2N-1} \omega^{-2kn}\, f^1[k] = \hat{f}_0^1[n] + \omega^{-n/2}\hat{f}_1^1[n], \tag{3.9}$$

$$\hat{f}_0^1[n] \triangleq \sum_{k=0}^{N-1} \omega^{-kn}\, f^1[2k] = \hat{f}^0[n], \quad \hat{f}_1^1[n] \triangleq \sum_{k=0}^{N-1} \omega^{-kn}\, f^1[2k+1].$$

According to the dyadic insertion rule and to the shift property Eq. (2.11) of the exponential splines, we get

$$f^1[2k+1] = S_0\left(k+\frac{1}{2}\right) = \frac{1}{N}\sum_{n=0}^{N-1} \frac{\hat{f}^0[n]}{u^p[n]}\,\zeta^p[n]\left(k+\frac{1}{2}\right), \tag{3.10}$$

$$\zeta^p[n]\left(k+\frac{1}{2}\right) = \omega^{kn}\,\omega^{n/2}\,\upsilon^p[n], \quad \upsilon^p[n] \triangleq \omega^{-n/2}\,\zeta^p[n]\left(\frac{1}{2}\right) = \sum_{l\in\mathbb{Z}} e^{\pi i l}\,\left(\frac{\sin\pi\,(n/N+l)}{\pi\,(n/N+l)}\right)^p. \tag{3.11}$$

Consequently,

$$f^1[2k+1] = \frac{1}{N}\sum_{n=0}^{N-1} \frac{\hat{f}^0[n]}{u^p[n]}\,\omega^{kn}\,\omega^{n/2}\,\upsilon^p[n] \Longrightarrow \hat{f}_1^1[n] = \omega^{n/2}\,\frac{\upsilon^p[n]}{u^p[n]}\,\hat{f}^0[n]. \tag{3.12}$$

By substituting Eq. (3.12) into Eq. (3.9), we get

$$\hat{f}^1[n]_1 = \hat{a}_0^p[n]\,\hat{f}^0[n], \text{ where } \hat{a}_0^p[n] \triangleq \frac{u^p[n]+\upsilon^p[n]}{u^p[n]} \tag{3.13}$$

$$f^1[k] = \frac{1}{2N}\sum_{k=0}^{2N-1} \omega^{kn/2}\,\hat{a}_0^p[n]\,\hat{f}^0[n]. \tag{3.14}$$

Thus, the fine array $\mathbf{f}^1$ is derived by p-filtering the initial data array $\mathbf{f}^0$ by the p-filter $\mathbf{a}_0^p$, whose frequency response $\hat{a}_0^p[n]$ is defined in Eq. (3.13).

Proposition 3.2 *If the order $p = 2r$ is even then the frequency response of the p-filter $\mathbf{a}_0^p$ is*

$$\hat{a}_0^{2r}[n] = 2\,\cos^{2r}\frac{\pi n}{2N}\,\frac{u_1^{2r}[n]}{u^{2r}[n]}, \quad n = 0, ..., 2N-1, \tag{3.15}$$

where $u_m^{2r}[n]$ are defined in Eq. (3.4).

Proof: Denote $A[n] \triangleq u^{2r}[n] + v^{2r}[n]$. By combining Eqs (3.8) and (3.11), we get

$$\hat{a}_0^{2r}[n] = \frac{A[n]}{u^{2r}[n]} = \sum_{l\in\mathbb{Z}} \left(1+e^{i\pi l}\right)\left(\frac{\sin\pi\,(n/N+l)}{\pi\,(n/N+l)}\right)^{2r} = \sum_{l\in\mathbb{Z}} \left(1+(-1^l)\right)\left(\frac{\sin\pi\,(n/N+l)}{\pi\,(n/N+l)}\right)^{2r}.$$

Thus, only even terms in the series are retained:

$$A[n] = 2\sum_{l\in\mathbb{Z}}\left(\frac{\sin 2\pi\,(n/2N+l)}{2\pi\,(n/2N+l)}\right)^{2r} = 2\sum_{l\in\mathbb{Z}}\left(\frac{\sin\pi\,(n/2N+l)\,\cos\pi\,(n/2N+l)}{\pi\,(n/2N+l)}\right)^{2r}$$

$$= 2\cos^{2r}\frac{\pi n}{2N}\sum_{l\in\mathbb{Z}}\left(\frac{\sin\pi\,(n/2N+l)}{\pi\,(n/2N+l)}\right)^{2r} = 2\cos^{2r}\frac{\pi n}{2N}\;u_1^{2r}[n].$$

■

Similarly to Eq. (3.13), we obtain a refinement expression from the resolution scale $m-1$:

$$\hat{f}^m[n]_m = \hat{a}^{2r}_{m-1}[n]\,\hat{f}^{m-1}[n]_{m-1}, \quad \hat{a}^{2r}_{m-1}[n] = 2\,\cos^{2r}\frac{\pi n}{N_m}\,\frac{u^{2r}_m[n]}{u^{2r}_{m-1}[n]}, \tag{3.16}$$

where $u^{2r}_m[n]$ are defined in Eq. (3.4) and $\quad n = 0, ..., N_m - 1$.

3.4 Computation of periodic splines at dyadic rational points

Once the samples $\left\{S(k) = f^0[k]\right\},\ k = 0, ..., N-1$ of a spline $S(t) \in {}^{2r}\mathcal{S}$ are available it follows from Eq. (3.16) that its values $\{S(k\,2^m)\},\ k \in \mathbb{Z}$, are derived by m successive refinement steps with the initial data $\mathbf{f}^0$ and filters $\mathbf{a}^{2r}_0$, $\mathbf{a}^{2r}_1$,...,$\mathbf{a}^{2r}_{m-1}$, whose frequency responseare given in Eq. (3.16). This process can be described explicitly. From Eq. (3.16) we get

$$\begin{aligned}
&\hat{f}^1[n]_1 = \hat{a}^{2r}_0[n]\,\hat{f}^0[n], \quad \hat{a}^{2r}_0[n] = 2\cos^{2r}\frac{\pi n}{2N}\,\frac{u^{2r}_{-1}[n]}{u^{2r}[n]}\,\hat{f}^0[n],\\
&\hat{f}^2[n]_2 = 2\,\cos^{2r}\frac{\pi n}{4N}\,\frac{u^{2r}_2[n]}{u^{2r}_1[n]}\hat{f}^1[n]_1 = 2^2\cos^{2r}\frac{\pi n}{4N}\,\cos^{2r}\frac{\pi n}{2N}\,\frac{u^{2r}_2[n]\,u^{2r}_1[n]}{u^{2r}_1[n]\,u^{2r}[n]}\hat{f}^0[n],\\
&\hat{f}^m[n]_m = 2^m\,\frac{u^{2r}_m[n]}{u^{2r}[n]}\hat{f}^0[n]\,\prod_{l=1}^{m}\cos^{2r}\frac{\pi n}{2^l N}.
\end{aligned} \tag{3.17}$$

Computation of the values $S(k/2^m) = f^m[k]$ of the spline $S(t) \in {}^{2r}\mathcal{S}$ from the samples $S(k) = f^0[k]$ is straightforward according to the following steps:

1. Calculate the $N-$point DFT $\hat{f}^0[n] = \sum_{k=0}^{N-1}\omega^{-kn}f^0[k]$ of the initial data $\mathbf{f}^0 = \left\{f^0[k]\right\}$.

2. Multiply the array $\left\{f^0[n]\right\}$

$$\hat{f}^m[n]_m = 2^m\,\frac{u^{2r}_m[n]}{u^{2r}[n]}\,\hat{f}^0[n]\,\prod_{l=1}^{\mu}\cos^{2r}\frac{\pi n}{2^l N}$$

   bearing in mind that $u^{2r}[n]$ and $\hat{f}^0[n]$ are $N-$periodic sequences, while $u^{2r}_m[n]$ is $2^m N-$periodic.

3. Implement the $2^m N-$point IDFT

$$S(k/2^m) = f^m[k] = \frac{1}{N_m}\sum_{n=0}^{N_m-1}\omega^{-2^m kn}\,\hat{f}^m[n]_m \tag{3.18}$$

   of the sequence $\hat{\mathbf{f}}^m = \left\{\hat{f}^m[n]_m\right\}$.

4 Ternary periodic subdivision

It was established in Section 3.4 that the values of even order splines at the dyadic rational points can be readily derived by Eq. (3.18) from the initial grid samples. This is not the case for splines of odd order. The

above dyadic subdivision scheme being applied to an odd order spline does not restore this spline but rather converges to a function that is smoother than the original spline ([23]). However, the ternary subdivision scheme to be presented restores values of splines of any order at the triadic rational points $\{3^{-m}k\}$, $m \in \mathbb{N}$.

4.1 Super-resolution spline spaces (triadic scale)

In this section $N = 2^j$, $j \in \mathbb{N}$, $\tilde{N}_m = 3^m N$, $m = 1, 2, ...,$ and $\omega \triangleq e^{2\pi i/N}$. The "triadic" DFT of an $\tilde{N}_m-$periodic signal $\mathbf{x} = \{x[k]\}$ is denoted as

$$\hat{x}[n]_{\tilde{m}} \triangleq \sum_{k=0}^{\tilde{N}_m-1} e^{-2\pi ink/\tilde{N}_m}\, x[k] = \sum_{k=0}^{\tilde{N}_m-1} \omega^{-3^m nk}\, x[k], \quad x[k] = \frac{1}{\tilde{N}_m} \sum_{n=0}^{\tilde{N}_m-1} \omega^{3^m nk}\, \hat{x}[n]_{\tilde{m}}.$$

We refine the spline space ${}^p\mathcal{S}$ along the triadic scale ${}^p\mathcal{S} = {}^p\tilde{\mathcal{S}}_0 \subset {}^p\tilde{\mathcal{S}}_1 \subset {}^p\tilde{\mathcal{S}}_2 ... \subset {}^p\tilde{\mathcal{S}}_m ...$, where ${}^p\tilde{\mathcal{S}}_m$ denotes the space of $N-$periodic splines of order p defined on the grid $\{3^{-m}\, k\}$, $k \in \mathbb{Z}$, $m = 0, 1, \ldots$.

The function $\tilde{\beta}^1_m(t)$ is defined to be zero outside the interval $(-3^{-m-1}, 3^{-m-1})$ and it is equal to 3^m inside the interval. The N-periodic normalized B-spline of first order on the grid $\{3^{-m}\, k\}$ and its Fourier coefficients are

$$\tilde{B}^1_m(t) \triangleq \sum_{k\in\mathbb{Z}} \tilde{\beta}^1_m\,(t + kN)\,, \quad c_n(\tilde{B}^1_m) = \frac{\sin \pi n/\tilde{N}_m}{\pi n/\tilde{N}_m}.$$

The N-periodic triadic normalized B-spline of order p is defined via the iterated circular convolution

$$\tilde{B}^p_m(t) \triangleq \tilde{B}^1_m \circledast \tilde{B}^{p-1}_m(t) = \frac{1}{N} \sum_{n\in\mathbb{Z}} \left(\frac{\sin(\pi n/\tilde{N}_m)}{\pi n/\tilde{N}_m} \right)^p e^{2\pi int/N}. \tag{4.1}$$

Each spline $S(t) \in {}^p\tilde{\mathcal{S}}_m$ is represented as

$$S(t) = \sum_{k=0}^{\tilde{N}_m-1} q[k]\tilde{B}^p_m\left(t - 3^{-m}k\right) = \frac{1}{\tilde{N}_m} \sum_{n=0}^{\tilde{N}_m-1} \xi[n]\, \tilde{\zeta}^p_m[n](t), \quad \xi[n] = \sum_{k=0}^{\tilde{N}_m-1} e^{-2\pi ink/\tilde{N}_m} q[k], \tag{4.2}$$

where the exponential splines, which form orthogonal bases of ${}^p\tilde{\mathcal{S}}_m$, are

$$\tilde{\zeta}^p_m[n](t) \triangleq \sum_{k=0}^{\tilde{N}_m-1} e^{2\pi ink/\tilde{N}_m} \tilde{B}^p_m(t - 3^{-m}k) = 3^m \sum_{l\in\mathbb{Z}} e^{2\pi i(n/N+3^m l)t} \left(\frac{\sin \pi(n/\tilde{N}_m + l)}{\pi(n/\tilde{N}_m + l)} \right)^p, \tag{4.3}$$

$n = 0, ..., \tilde{N}_m - 1$. The $\tilde{N}_m$ -periodic characteristic sequence of the space ${}^p\tilde{\mathcal{S}}_m$ is

$$\tilde{u}^p_m[n] \triangleq \tilde{\zeta}^p_m[n](0) = \sum_{k=0}^{\tilde{N}_m-1} e^{2\pi ink/\tilde{N}_m} \tilde{B}^p_m(3^{-m}k) = 3^m \sum_{l\in\mathbb{Z}} \left(\frac{\sin \pi(n/\tilde{N}_m + l)}{\pi(n/\tilde{N}_m + l)} \right)^p. \tag{4.4}$$

Proof of the following fact is similar to the proof of Proposition 3.1.

Proposition 4.1 *The characteristic sequence $\tilde{u}^p_m[n]$ of the space ${}^p\tilde{\mathcal{S}}_m$ can be calculated via the $3^m N-$point DFT of the sampled B-spline $B^p(t) \in {}^p\mathcal{S}$ is*

$$\tilde{u}^p_m[n] = 3^m\, \hat{b}^p[n]_{\tilde{m}} = 3^m \sum_{k=0}^{\tilde{N}_m-1} \omega^{-3^m kn}\, B^p(k). \tag{4.5}$$

The spline $S(t) \in {}^p\tilde{\mathcal{S}}_m$, which interpolates an $\tilde{N}_m$ -periodic signal $\mathbf{x} = \{x[k]\}$: $S(k/3^m) = x[k],\ k \in \mathbb{Z}$, is

$$S(t) = \frac{1}{\tilde{N}_m} \sum_{n=0}^{\tilde{N}_m - 1} \frac{\hat{x}[n]_{\tilde{m}}}{\tilde{u}_m^p[n]}\, \tilde{\zeta}_m^p[n](t), \quad \hat{x}[n]_{\tilde{m}} \triangleq \sum_{k=0}^{\tilde{N}_m - 1} \omega^{-3^m nk} x[k]. \tag{4.6}$$

4.2 Insertion rule

Calculation of the values at triadic rational points of N-periodic splines of order p is implemented via the following refinement steps.

Triadic periodic spline insertion rule: *Assume we have a spline $S_0(t) \in {}^p\mathcal{S}$ and $\mathbf{f}^0 \triangleq \left\{f^0[k] = S_0(k)\right\}$, $k \in \mathbb{Z}$. For $m = 1, 2, \ldots$, we construct on the grid $\tilde{\mathbf{g}}^{m-1} \triangleq \left\{k/3^{m-1}\right\},\ k \in \mathbb{Z}$, a spline $S_{m-1}(t) \in {}^p\tilde{\mathcal{S}}_{m-1}$, $S_{m-1}\left(k/3^{m-1}\right) = f^{m-1}[k],\ k \in \mathbb{Z}$, which interpolates the sequence $\mathbf{f}^{m-1} \triangleq \left\{f^{m-1}[k]\right\}$. Then, $f^m[k] \triangleq S_{m-1}\left(k/3^m\right),\ k \in \mathbb{Z}$.*

In other words, in order to refine the data $\mathbf{f}^{m-1}$ from the grid $\left\{k/3^{m-1}\right\}$ to the grid $\{k/3^m\}$, we construct the spline $S_{m-1}(t)$, which interpolates $\mathbf{f}^{m-1}$ on the grid $\left\{k/3^{m-1}\right\}$ and define $f^m[3k] = f^{m-1}[k]$ and $f^m[3k \pm 1] = S_{m-1}((k \pm 1/3)/3^{m-1})$ that are the values of the spline at points around the interpolation points.

This insertion rule reproduces a spline of any order, which means that $S_m(t) \equiv S_{m-1}(t) \equiv \ldots \equiv S_0(t)$. Consequently, each refinement step provides the values of the spline $S_0(t)$ at the subsequent set of triadic rational points.

The proof of this fact for splines of even order is similar to the proof of Proposition 3.1.

4.3 Periodic spline filters for triadic subdivision

The spline $S_0(t) \in {}^p\tilde{\mathcal{S}}$ ($S(k) = f^0[k],\ k \in \mathbb{Z}$,) which interpolates the N-periodic sequence $\mathbf{f}^0 \triangleq \left\{f^0[k]\right\}$ is represented by

$$S_0(t) = \frac{1}{N} \sum_{n=0}^{N/2-1} \frac{\hat{f}^0[n]}{u^p[n]}\, \zeta^p[n](t), \quad \zeta^p[n](t) = \sum_{l \in \mathbb{Z}} e^{2\pi i (n/N + l)t} \left(\frac{\sin \pi\,(n/N + l)}{\pi\,(n/N + l)}\right)^p.$$

The DFT of the refined array

$$\begin{aligned} &\hat{f}^1[n]_{\tilde{1}} = \hat{f}_0^1[n] + e^{-2\pi i n/3N} \hat{f}_1^1[n] + e^{2\pi i n/3N} \hat{f}_{-1}^1[n], \\ &\hat{f}_0^1[n] \triangleq \sum_{k=0}^{N-1} \omega^{-kn}\, f^1[3k] = \hat{f}^0[n], \quad \hat{f}_{\pm 1}^1[n] \triangleq \sum_{k=0}^{N-1} \omega^{-kn}\, f^1[3k \pm 1]. \end{aligned} \tag{4.7}$$

According to the triadic insertion rule and to the shift property Eq. (2.11) of the exponential splines, we

get

$$f^1[3k \pm 1] = S_0\left(k \pm \frac{1}{3}\right) = \frac{1}{N}\sum_{n=0}^{N-1} \frac{\hat{f}^0[n]}{u^p[n]}\,\zeta^p[n]\left(k \pm \frac{1}{3}\right) \tag{4.8}$$

$$\zeta^p[n]\left(k \pm \frac{1}{3}\right) = \omega^{kn}\, e^{\pm 2\pi i n/3N}\, \upsilon^p_{\pm}[n], \quad \text{where}$$

$$\upsilon^p_{\pm}[n] \triangleq e^{\mp 2\pi i n/3N}\,\zeta^p[n]\left(\frac{1}{3}\right) = \sum_{l\in\mathbb{Z}} e^{\pm 2\pi i l/3}\,\left(\frac{\sin\pi\,(n/N+l)}{\pi\,(n/N+l)}\right)^p. \tag{4.9}$$

Consequently,

$$f^1[3k \pm 1] = \frac{1}{N}\sum_{n=0}^{N-1} \frac{\hat{f}^0[n]}{u^p[n]}\,\omega^{kn}\, e^{\pm 2\pi i n/3N}\,\upsilon^p_{\pm}[n] \Longrightarrow \hat{\mathbf{f}}^1_{\pm 1}[n] = e^{\pm 2\pi i n/3N}\frac{\upsilon^p_{\pm}[n]}{u^p[n]}\,\hat{f}^0[n]. \tag{4.10}$$

Substituting Eq. (4.10) into Eq. (4.7), we get

$$\hat{f}^1[n]_{\tilde{1}} = \hat{a}^p_0[n]\,\hat{f}^0[n], \text{ where } \hat{a}^p_0[n] \triangleq \frac{u^p[n] + \upsilon^p_1[n] + \upsilon^p_{-1}[n]}{u^p[n]} \quad f^1[k] = \frac{1}{3N}\sum_{k=0}^{3N-1} \omega^{kn/3}\,\hat{a}^p_0[n]\,\hat{f}^0[n]. \tag{4.11}$$

Equation (4.11) means that the refined array $\mathbf{f}^1$ is derived by p-filtering of the initial array $\mathbf{f}^0$ with the p-filter $\mathbf{a}^p_0$, whose frequency response is $\{\hat{a}^p_0[n]\}$.

Proposition 4.2 *The frequency response of the p-filter $\mathbf{a}^p_0$ for splines of order p is*

$$\hat{a}^p_0[n] = 3^{-p}\left(1 + 2\cos\frac{2\pi n}{3N}\right)^p \frac{\tilde{u}^p_1[n]}{u^p[n]}, \quad n = 0, ..., 3N-1, \tag{4.12}$$

where the characteristic sequences $\tilde{u}^p_m[n]$ are defined in Eq. (4.4).

Proof: Denote $A[n] \triangleq u^p[n] + \upsilon^p_1[n] + \upsilon^p_{-1}[n]$. Combining Eqs. (2.14) and (4.9), we get

$$\hat{a}^p_0[n] = \frac{A[n]}{u^p[n]} = \sum_{l\in\mathbb{Z}}\left(1 + e^{2\pi i l/3} + e^{-2\pi i l/3}\right)\left(\frac{\sin\pi\,(n/N+l)}{\pi\,(n/N+l)}\right)^p$$

$$= \sum_{l\in\mathbb{Z}}\left(1 + 2\cos\frac{2\pi l}{3}\right)\left(\frac{\sin\pi\,(n/N+l)}{\pi\,(n/N+l)}\right)^p.$$

Thus, only the terms $l = 3\nu$, $\nu \in \mathbb{Z}$, in the series are retained:

$$A[n] = 3\sum_{l\in\mathbb{Z}}\left(\frac{\sin 3\pi\,(n/3N+l)}{3\pi\,(n/3N+l)}\right)^{2r}.$$

Using the trigonometric identity $\sin 3\alpha = \sin\alpha(1 + 2\cos 2\alpha)$, we get

$$A[n] = 3^{1-p}\sum_{l\in\mathbb{Z}}\left(\frac{\sin\pi\,(n/3N+l)\,(1 + 2\cos\pi\,(2n/3N+2l)}{\pi\,(n/2N+l)}\right)^p$$

$$= 3^{1-p}\left(1 + 2\cos\frac{2\pi n}{3N}\right)^p\sum_{l\in\mathbb{Z}}\left(\frac{\sin\pi\,(n/3N+l)}{\pi\,(n/3N+l)}\right)^p = \frac{1}{3^p}\,\left(1 + 2\cos\frac{2\pi n}{3N}\right)^p\,\tilde{u}^p_1[n].$$

■

Corollary 4.1 *The DFT of the m-th refined array of splines of order p is*

$$\hat{f}^m[n]_{\tilde{m}} = \hat{a}^p_{m-1}[n]\,\hat{f}^{m-1}[n]_{\widetilde{m-1}}, \quad \hat{a}^p_{m-1}[n] = \frac{1}{3^p}\left(1+2\cos\frac{2\pi n}{\tilde{N}_m}\right)^p \frac{\tilde{u}^p_m[n]}{\tilde{u}^p_{m-1}[n]}, \tag{4.13}$$

where $\tilde{u}^p_m[n]$ *are defined in Eq. (4.4),* $\tilde{N}_m = N\,3^{-m}, \quad n = 0, ..., \tilde{N}_m - 1.$

4.4 Computation of periodic splines at triadic rational points

Now we are in a position to justify the claim about restoration of splines by the ternary subdivision.

Theorem 4.1 *Let* $S_0(t) \in {}^p\mathcal{S}$ *be an N-periodic spline of order p with nodes on the grid* $\{k\}$, $k \in \mathbb{Z}$, *and its samples are* $\left\{S(k) = f^0[k]\right\}$, $k \in \mathbb{Z}$. *The sequence* $\mathbf{f}^0 \triangleq \left\{f^0[k]\right\}$, $k \in \mathbb{Z}$ *is N-periodic. Then, all the subsequent subdivision steps with the triadic periodic spline insertion rule reproduce the values of this spline*

$$f^m[k] = S(k/3^m), \quad k \in \mathbb{Z},\ m = 1, 2, ..., . \tag{4.14}$$

Proof: From the definition of the triadic insertion rule we have $S_0(k/3) = f^1[k]$. The next subdivision step consists of spline $S_1(t) \in {}^p\tilde{\mathcal{S}}_1$ construction on the grid $\mathbf{g}^1 = \{k/3\}$ such that $S_1(k/3) = f^1[k]$. Then, $f^2[k] = S_1(k/9)$. We prove that $f^2[k] = S_0(k/9)$. The subsequent relations in Eq. (4.14) are derived by a simple induction.

The array $\mathbf{f}^2$ is obtained by successive application of the filters $\mathbf{a}^p_1$ after $\mathbf{a}^p_0$ to the array $\mathbf{f}^0$:

$$\begin{aligned}\hat{f}^2[n]_{\tilde{2}} &= \hat{a}^p_1[n]\,\hat{f}^1[n]_{\tilde{1}} = \hat{a}^p_1[n]\,\hat{a}^p_0[n]\,\hat{f}^0[n] \\ &= \frac{1}{3^{2p}}\left(1+2\cos\frac{2\pi n}{9N}\right)^p \frac{\tilde{u}^p_2[n]}{\tilde{u}^p_1[n]}\left(1+2\cos\frac{2\pi n}{3N}\right)^p \frac{\tilde{u}^p_1[n]}{u^p[n]}\ \hat{f}^0[n] = \hat{H}[n]\,\frac{\hat{f}^0[n]}{u^p[n]}.\end{aligned} \tag{4.15}$$

where

$$\hat{H}[n] \triangleq \frac{1}{3^{2p}}\left(1+2\cos\frac{2\pi n}{9N}\right)^p \left(1+2\cos\frac{2\pi n}{3N}\right)^p \tilde{u}^p_2[n]. \tag{4.16}$$

Denote $\mathbf{s} \triangleq \{s[k] = S_0(k/9)\}$, $k \in \mathbb{Z}$. Similarly to Eq.(4.7), the $9N$-point DFT of this array is represented by

$$\hat{s}[n]_{\tilde{2}} = \sum_{k=0}^{9N-1} e^{-2\pi i n k/9N} s[k] = \hat{s}_0(n) + \sum_{l=1}^{4}\left(e^{-2\pi i l n/9N}\hat{s}_l[n] + e^{2\pi i l n/9N}\hat{s}_{-l}[n]\right), \tag{4.17}$$

where $\hat{s}_0(n) \triangleq \sum_{k=0}^{N}\omega^{-nk}S_0(k) = \hat{f}_0(n)$ and for $l = \pm1, \pm2, \pm3, \pm4$ we get

$$\begin{aligned}\hat{s}_l[n] &\triangleq \sum_{k=0}^{N}\omega^{-nk}S_0\left(k+\tfrac{l}{9}\right) = \sum_{k=0}^{N}\omega^{-nk}\tfrac{1}{N}\sum_{\nu=0}^{N-1}\tfrac{\hat{f}^0[\nu]}{u^p[\nu]}\,\zeta^p[\nu]\left(k+\tfrac{l}{9}\right) \\ &= \sum_{k=0}^{N}\omega^{-nk}\tfrac{1}{N}\sum_{\nu=0}^{N-1}\omega^{\nu k}\tfrac{\hat{f}^0[\nu]}{u^p[\nu]}\,\zeta^p[\nu]\left(\tfrac{l}{9}\right) \\ &= \sum_{k=0}^{N}\omega^{-nk}\tfrac{1}{N}\sum_{\nu=0}^{N-1}\omega^{\nu k}\tfrac{\hat{f}^0[\nu]}{u^p[\nu]}\,e^{2\pi i l\nu/9N}\zeta^p[\nu]\,\tilde{v}^p[n] = \tfrac{\hat{f}^0[n]}{u^p[n]}\,e^{2\pi i l n/9N}\,v^p_l[n].\end{aligned}$$

The sequence $\tilde{v}^p_l[n]$ is

$$\tilde{v}^p_l[n] \triangleq e^{-2\pi i l n/9N}\zeta^p[n]\left(\frac{l}{9}\right) = \sum_{\nu\in\mathbb{Z}} e^{2\nu l\pi i/9}\left(\frac{\sin\pi\,(n/N+\nu)}{\pi\,(n/N+\nu)}\right)^p. \tag{4.18}$$

By substituting Eq. (4.18) into Eq. (4.17), we get

$$\begin{aligned}\hat{s}[n] &= \hat{f}^0[n]\,\frac{u^p[n]+\sum_{l=1}^{4}\left(\tilde{v}_l^p[n]+\tilde{v}_{-l}^p[n]\right)}{u^p[n]} \\ &= \frac{\hat{f}^0[n]}{u^p[n]}\sum_{\nu\in\mathbb{Z}}\left(1+\sum_{l=1}^{4}\left(e^{2\nu l\pi i/9}+e^{-2\nu l\pi i/9}\right)\right)\left(\frac{\sin\pi\,(n/N+\nu)}{\pi\,(n/N+\nu)}\right)^p \\ &= \frac{\hat{f}^0[n]}{u^p[n]}\sum_{\nu\in\mathbb{Z}}\left(1+2\sum_{l=1}^{4}\cos\frac{2\nu l\pi}{9}\right)\left(\frac{\sin\pi\,(n/N+\nu)}{\pi\,(n/N+\nu)}\right)^p.\end{aligned} \tag{4.19}$$

It is readily verified that if $\nu = 9n$ $1+2\sum_{l=1}^{4}\cos 2\nu l\pi/9 = 9$ and zero otherwise. Thus,

$$\begin{aligned}\hat{s}[n] &= \frac{9\hat{f}^0[n]}{u^p[n]}\sum_{\nu\in\mathbb{Z}}\left(\frac{\sin 9\pi(n/9N+\pi\nu)}{9(n/9N+\pi\nu)}\right)^p = 9^{1-p}\left(1+2\cos\tfrac{2\pi n}{9N}\right)^p\ \frac{\hat{f}^0[n]}{u^p[n]}\sum_{\nu\in\mathbb{Z}}\left(\frac{\sin 3\pi(n/9N+\pi\nu)}{9(n/9N+\pi\nu)}\right)^p \\ &= 9^{1-p}\left(1+2\cos\tfrac{2\pi n}{9N}\right)^p\ \left(1+2\cos\tfrac{2\pi n}{3N}\right)^p\ \frac{\hat{f}^0[n]}{u^p[n]}\sum_{\nu\in\mathbb{Z}}\left(\frac{\sin\pi(n/9N+\pi\nu)}{9(n/9N+\pi\nu)}\right)^p \\ &= 9^{-p}\left(1+2\cos\tfrac{2\pi n}{9N}\right)^p\ \left(1+2\cos\tfrac{2\pi n}{3N}\right)^p\ \tilde{u}_2^p[n]\ \frac{\hat{f}^0[n]}{u^p[n]}.\end{aligned} \tag{4.20}$$

By comparing Eq. (4.20) with Eqs. (4.15) and (4.16), we see that $\hat{f}^2[n] = \hat{\mathbf{s}}[n],\ n = 0,...,9N-1$ and, consequently, $f^2[k] = S(k/9),\ k\in\mathbb{Z}$. Repeating the above reasoning with the initial data set $\mathbf{f}^1$ instead of using $\mathbf{f}^0$, we prove that $f^3[k] = S_1(k\,3^{-3})$ and so on. ■

4.5 Practical implementation

It follows from Theorem 4.1 that, once we know the samples $\left\{S(k) = f^0[k]\right\},\ k\in\mathbb{Z}$ of a spline $S(t)\in{}^p\mathcal{S}$, its values $\left\{S(k\,3^m)\right\},\ k\in\mathbb{Z},\ m = 1,2,...,$ are derived by m successive refinement steps with the initial data $\mathbf{f}^0$ and the filters $\mathbf{a}_0^p$, $\mathbf{a}_1^p$,...,$\mathbf{a}_{m-1}^p$, whose frequency responses are given in Eq. (4.13). This process can be described explicitly. Due to Eq. (4.13), we get

$$\hat{f}^m[n]_{\tilde{m}} = \frac{\tilde{u}_m^p[n]}{3^{mp}\,u^p[n]}\,\hat{f}^0[n]\,\prod_{l=1}^{m}\left(1+2\cos\frac{2\pi n}{\tilde{N}_{-l}}\right)^p. \tag{4.21}$$

The values computation of $S(k/3^m) = f^m[k]$ of the spline $S(t)\in{}^p\mathcal{S}$ from the samples $S(k) = f^0[k]$ is done straightforward:

1. Calculate the $N-$point DFT $\hat{f}^0[n] = \sum_{k=0}^{N-1}\omega^{-kn}\,f^0[k]$ of the initial data $\mathbf{f}^0 = \left\{f^0[k]\right\}$.
2. Derive $\hat{f}^m[n]_{\tilde{m}}$ from Eq. (4.21) bearing in mind that $u^p[n]$ and $\hat{f}^0[n]$ are $N-$periodic sequences, while $\tilde{u}_m^p[n]$, which are calculated according to Proposition 4.1, is 3^mN-periodic.
3. Implement the 3^mN-point IDFT $S(k/3^m) = f^m[k] = \frac{1}{3^mN}\sum_{n=0}^{3^mN-1}e^{-2\pi ikn/3^mN}\,\hat{f}^m[n]_{\tilde{m}}$ of the sequence $\hat{\mathbf{f}}^m = \left\{\hat{f}^m[n]_{\tilde{m}}\right\}$.

4.6 Two-dimensional spline subdivision

The subdivision schemes, which provide internal values for 1D splines, are extended to 2D cases in a natural way. A two-dimensional N-periodic spline $S(x,y)\triangleq\sum_{k,n=0}^{N-1}s[k,n]\,B^p(x-k)\,B^q(y-n)$ from the space ${}^{p,q}\mathcal{S}$ is a 1D spline of order p with respect to x when the variable y is fixed and a 1D spline of order q with respect

to y when the variable x is fixed. Therefore, for the grid samples of the spline $\{S(k,n)\}$, $k,n=0,...,N-1$, we can first apply a dyadic (for this $p=2r$) or a triadic 1D subdivision scheme to the columns of the array $\{S(k,n)\}$ thus producing one of the two arrays

$$\mathbf{s}_m^P = \{S(k/P^m, n]\}, \ k=0,...,P^m N-1, \ n=0,...,N-1, \ P=2 \text{ or } 3.$$

The next step is an application of a subdivision algorithm to the rows of the array $\mathbf{s}_m^P$, $P=2$ or $P=3$, thus producing one of the following four arrays:

$$\left\{S(k/P^m, n/Q^l]\right\}, \ k=0,...,P^m N-1, \ n=0,...,Q^l N-1, \ P=2 \text{ or } 3, \ Q=2 \text{ or } 3,$$

and m and l are natural numbers.

We emphasize that a spline $S(x,y)$ can have different orders with respect to x and y. The subdivision algorithms and their depth can be different for the columns and for the rows. In a MATLAB implementation, calculations for periodic splines are accelerated because basic operations such as the fast Fourier transforms, multiplications and divisions are applicable to the whole array rather than to separate columns and rows.

5 Upsampling signals and images

An obvious application for 1D and 2D spline subdivision is in upsampling discrete-time signals and digital images.

5.1 Upsampling discrete-time signals

If a signal $\mathbf{x}=\{x[k]\}$, $k=0,...,N-1$, consists of samples of a smooth periodic function $x[k]=f(k/T)$, the subdivision techniques presented in Sections 3 and 4 enable us to closely approximate the function on the internal points even if the grid $\{k/T\}$ is sparse. When the available samples are affected by noise, then smoothing splines do a good restoration job. If the function $f(t)$ is bandlimited (a trigonometric polynomial) then it is almost perfectly restored by the higher order interpolating splines.

Example 1: Restoration of a bandlimited signal. The 1-periodic function
$f(t) \triangleq \cos 2\pi Ft + 5\sin \pi Ft - 2 * \sin 4\pi Ft - \cos \pi Ft/2, \quad F=32$, is displayed in Fig. 5.1.

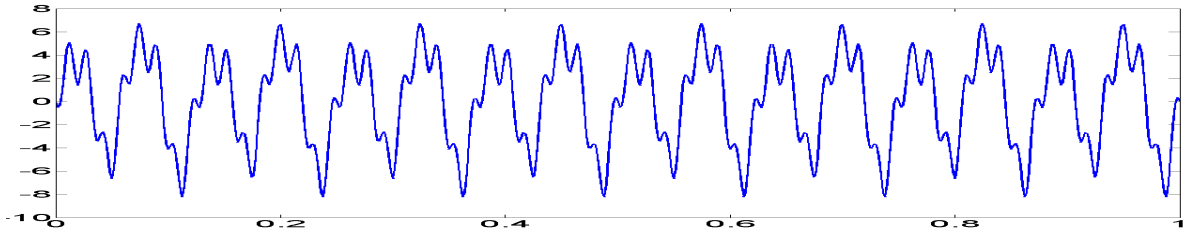

Figure 5.1: The function $f(t)$

The function is sampled on the grid $\{k/256\}$. The signal $\mathbf{f}^0 \triangleq \{f(k/256)\}$, $k = 0, ..., 255$, is used as the initial data. We compared the performances of the subdivision schemes with splines of different orders for restoration of the function $f(t)$ at dyadic and triadic rational points. As expected, the high order splines achieved the best result. The left panel in Fig. 5.2 illustrates the results from the application of the dyadic subdivision of 6 steps of the splines $S^{2r}(t)$ of even orders ranging from 2 to 20, which interpolate the signal $\mathbf{f}^0$. The subdivision produces the splines $S^{2r}(k/2^{14})$ values. Thus, the signal $\mathbf{f}^0$ is upsampled at the ratio 1:64. The results are evaluated by the averaged deviations $d^{2r} \triangleq \sqrt{2^{-14}\sum_{k=0}^{2^{14}-1}|f(k/2^{14}) - S^{2r}(k/2^{14})|}$. The bars in the left panel display the values $D^{2r} \triangleq \log_{10}(d^{2r})$. The best restoration of the function f is achieved by the 16-th order spline where $D^{16} = -7.39$.

The splines $S^{2r+1}(t)$ of odd orders ranging from 3 to 21 are restored by the ternary subdivision of four steps. The subdivision produces the splines values $S^{2r+1}(k/K)$, $K = 256 \cdot 3^4 = 20736$. Thus, the signal $\mathbf{f}^0$ is upsampled at the ratio 1:81. The results are evaluated by the averaged deviations $d^{2r+1} \triangleq \sqrt{K^{-1}\sum_{k=0}^{K-1}|f(k/K) - S^{2r}(k/K)|}$. The bars in the right panel display the values $D^{2r+1} \triangleq \log_{10}(d^{2r+1})$. The best restoration result of the function f is achieved by the 17-th order spline where $D^{17} = -7.5$.

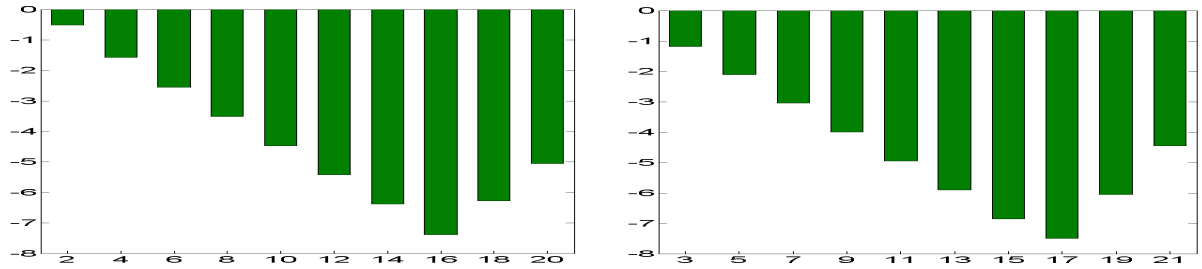

Figure 5.2: Left: X-axis – orders of the splines. Y-axis – logarithmic deviations D^{2r} of the splines S^{2r} from the function f (dyadic subdivision). Right: X-axis – orders of the splines. Y-axis – logarithmic deviations D^{2r+1} of the splines S^{2r+1} from the function f (ternary subdivision)

Example2: Restoration of a noised signal . In this example, the original signal is a fragment of the *chirp* function $f(t) = \sin(1/t)$, where $t \in [0.071, 0.971]$. This fragment is displayed in Fig. 5.3. It oscillates with a frequency variable.

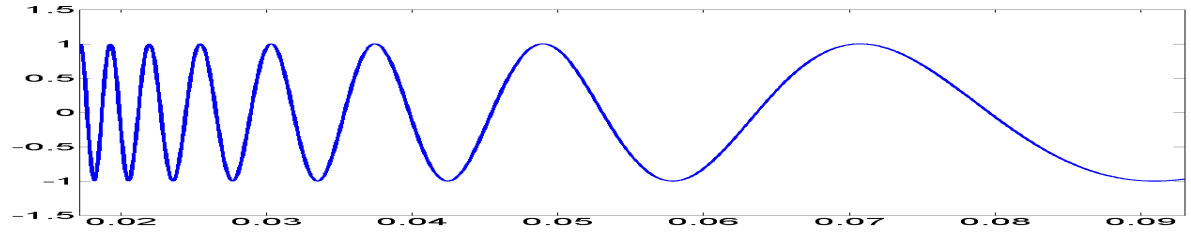

Figure 5.3: The *chirp* function $f(t) = \sin(1/t)$

In the first experiment, the data contains 128 equidistant samples of the function, which were affected by white noise whose STD=0.35. These data were upsampled at ratio 1:8 by subdivision with the smoothing spline of orders 4, 8 and 12, where the results are displayed in the top, middle and bottom of the left side of Fig. 5.4, respectively. In the second experiment, the data was decimated by factor of 2, thus, the initial data consisted of 64 noised samples. These data were upsampled at the ratio 1:16 by the application of subdivision with the smoothing spline of orders 4, 8 and 12 described in the right side of Fig. 5.4, respectively.

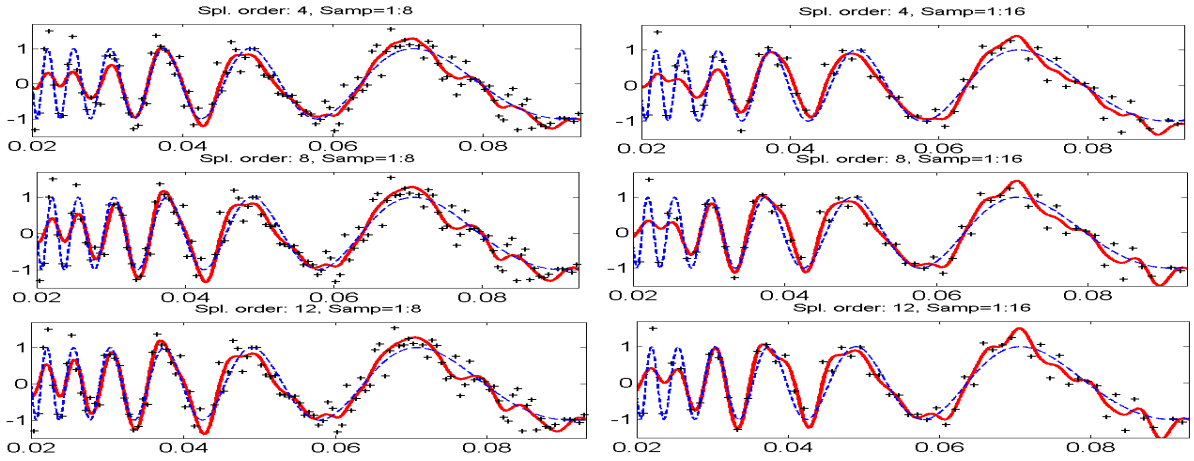

Figure 5.4: Left: X-axis – orders of the splines. Y-axis – logarithmic deviations D^{2r} of splines S^{2r} from the function f (dyadic subdivision). Right: X-axis – orders of the splines. Y-axis – logarithmic deviations D^{2r+1} of splines S^{2r+1} from the function f (ternary subdivision).

We observe that, in spite of the presence of strong noise and low-rate sampling, the original signal was satisfactorily restored. Note that order 4 (cubic) splines best restore the low-frequency part of the signalwhile the splines of 12th order restore well the high-frequency region.

5.2 Upsampling digital images

Upsampling an image using 2D interpolating splines increases its resolution. For this, the image pixels are treated as the grid samples of a 2D spline and the initial data array is upsampled by the spline's values in internal points, which are derived by the application of dyadic or ternary subdivision as it is described in Sections 3.4 and 4.5, respectively. The 2D subdivision is outlined in Section 4.6. When the pixels of the image are affected by noise, the smoothing splines provide a good approximation.

We illustrate the performance of the spline subdivision schemes in a few experiments with the benchmark images "Lena" and "Barbara", which are 512×512 pixels arrays denoted by $\mathbf{L}$ and $\mathbf{B}$, respectively.

Example 1: Restoration of the "Lena" image from downsampled arrays. In this example, the "Lena" image is restored after it was decimated by ratio 2:1 and 4:1 to generate the data arrays $\mathbf{d}_2$ of size

256×256 and $\mathbf{d}_4$ of size 128×128. The low-pass anti-aliasing filtering was not applied to the decimated arrays. The available data arrays $\mathbf{d}_s,\ s=2,4$ were interpolated by the even order splines $S_s^{2r}(x,y),\ s=2,4$, that is $S_s^{2r}(k,n)=d_s[k,n]$. Then, the original array was restored by the splines values $L(k,n)\approx S_2^{2r}(k/2,n/2)$ and $L(k,n)\approx S_4^{2r}(k/4,n/4)$, $k,n,=0,,,,,511$.

The proximity between the restored image $\tilde{\mathbf{L}}$ and the original image $\mathbf{L}$ is evaluated visually and by the Peak-Signal-to-Noise ratio (PSNR)

$$PSNR \triangleq 10\log_{10}\left(\frac{M\,255^2}{\sum_{k=1}^{M}(x_k-\tilde{x}_k)^2}\right)\ dB$$

where M is the number of pixels in the image (in our experiments, $M=512^2$), $\{x_k\}_{k=1}^{M}$ are the original pixels of the image $\mathbf{L}$ and $\{\tilde{x}_k\}_{k=1}^{M}$ are the pixels of the image $\tilde{\mathbf{L}}$.

It turns out that the best PSNR was achieved by using subdivision with the cubic splines. Figure 5.5 displays the results of this restoration. We observe that the restoration from the array $\mathbf{d}_2$ is quite satisfactory (PSNR=33.28), while the restoration from the array $\mathbf{d}_4$ is somewhat blurred (PSNR=27.25).

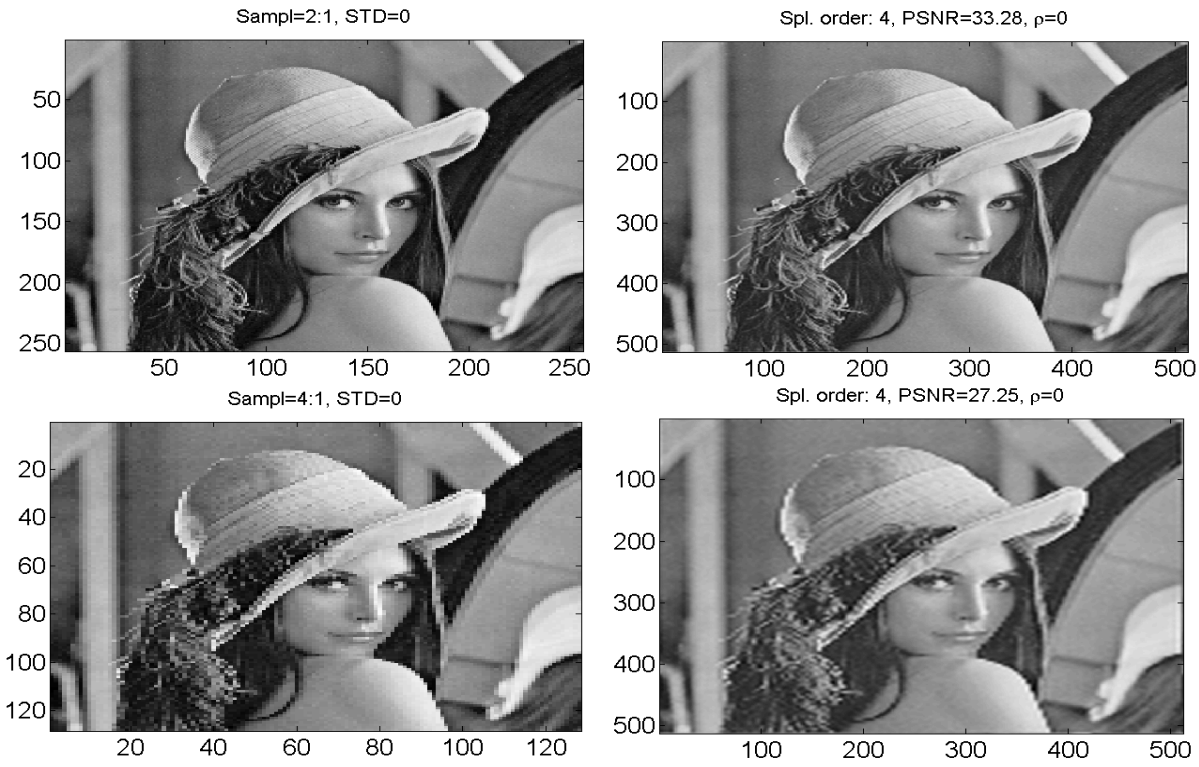

Figure 5.5: Left: Decimated data arrays. Top: $\mathbf{d}_2$, bottom $\mathbf{d}_4$, "Lena" image restored by the interpolating cubic splines subdivision from $\mathbf{d}_2$ (top) and $\mathbf{d}_4$ (bottom)

Example 2: Restoration of the "Lena" image from noised decimated arrays. In this example, the "Lena" image was decimated by factors of 2:1 and 4:1 to generate the data arrays $\mathbf{d}_2$ of size 256×256

and $\mathbf{d}_4$ of size 128×128, respectively. Then, they were corrupred by a strong Gaussian noise whose was STD=20. The data arrays $\mathbf{d}_s$, $s = 2, 4$ were approximated by the even order splines $S^{2r}_{\rho,s}(x, y)$, $s = 2, 4$, that is $S^{2r}_{\rho,s}(k, n) = d_s[k, n]$, where the optimal values of the parameter ρ were derived from Eq. (2.35). Then, the original array was restored by the splines $L(k, n) \approx S^{2r}_{\rho,2}(k/2, n/2)$ and $L(k, n) \approx S^{2r}_{\rho,4}(k/4, n/4)$, $k, n, = 0, \ldots, 511$. As before, the best PSNR was produced by the subdivision with cubic splines. Figure 5.6 displays the results of this restoration. We observe that the noise is suppressed in the restored images from the array $\mathbf{d}_2$ (PSNR=26.75), while the restoration from the array $\mathbf{d}_4$ is blurred (PSNR=24.35).

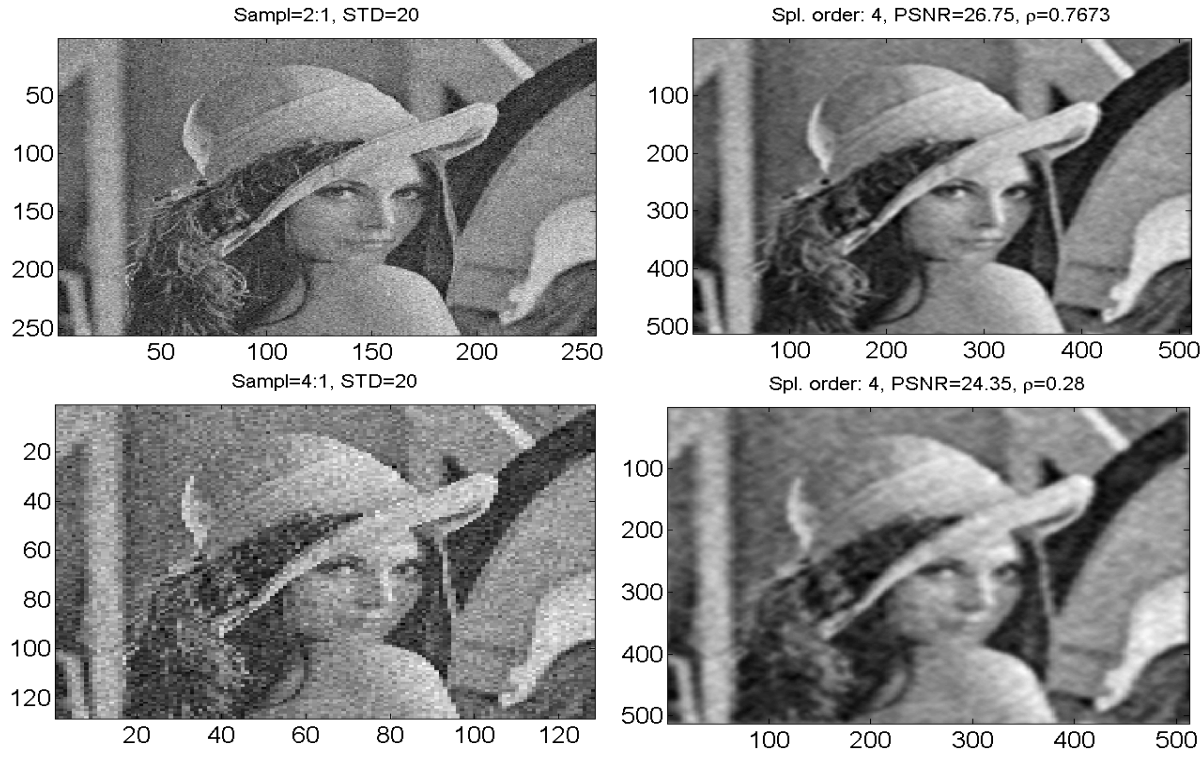

Figure 5.6: Left: Decimated *noised* images. Top: $\mathbf{d}_2$, bottom $\mathbf{d}_4$. Right: "Lena" image restored by the interpolating cubic splines subdivision from $\mathbf{d}_2$ (top) and from $\mathbf{d}_4$ (bottom)

Example 3: Upsampling the "Barbara" image. In this example, we upsample the "Barbara" image of size 512×512. It is given in the array $\mathbf{B}$ of pixels. We used the 2D spline $S^{7,8}(x, y)$,, which interpolates the initial data, that is $S^{7,8}(k, n) = B[k, n]$. The spline $S^{7,8}(x, y)$ is of order 7 in the vertical direction and order 8 in the horizontal direction. By the application of 3 steps of the ternary subdivision in the vertical direction and 4 steps of the dyadic subdivision in the horizontal direction, we generate the array $\mathbf{S} \triangleq \left\{S^{7,8}(k/27, n/16)\right\}$, where $k = 0, \ldots, 13823$ and $n = 0, \ldots, 8191$. The array $\mathbf{S}$ is used for the upsampled image. The result is displayed in Fig. 5.7. We see that the upsampling significantly increased the image resolution.

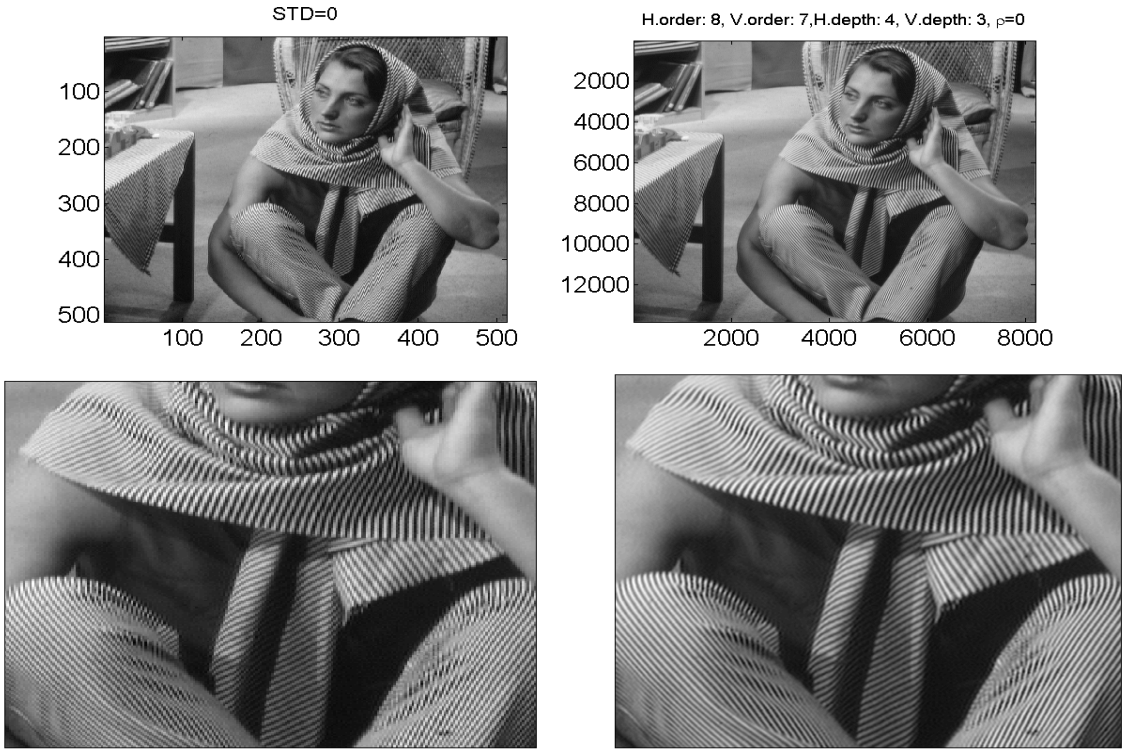

Figure 5.7: Left: Original "Barbara" image in two formats. Top: The whole image. Bottom: A fragment of the image. Right: the upsampled image upsampled after the application of the interpolating splines $S^{7,8}(x,y)$ using ternary subdivision in the vertical direction and dyadic subdivision in the horizontal direction

Example 4: Upsampling the "Barbara" image that was corrupted by noise. In this example, the pixels array $\mathbf{B}$ is corrupted by a moderate Gaussian noise with STD=10. We upsample the image by using the 2D bicubic smoothing spline $S^{4,4}_{\rho}(x,y)$, which approximates the original noised data, that is $S^{4,4}_{\rho}(k,n) \approx B[k,n]$. The optimal value of the parameter ρ was derived from Eq. (2.35). By the application of 3 steps of the ternary subdivision in either direction, we generated the array $\mathbf{S}_{\rho} \stackrel{\triangle}{=} \left\{S^{4,4}_{\rho}(k/9, n/9)\right\}$, $k,n = 0,\ldots,4607$. The array $\mathbf{S}_{\rho}$ is used as the upsampled image. The upsampling result is displayed in Fig. 5.8. We observe that the upsampling suppressed the noise and increased the image resolution.

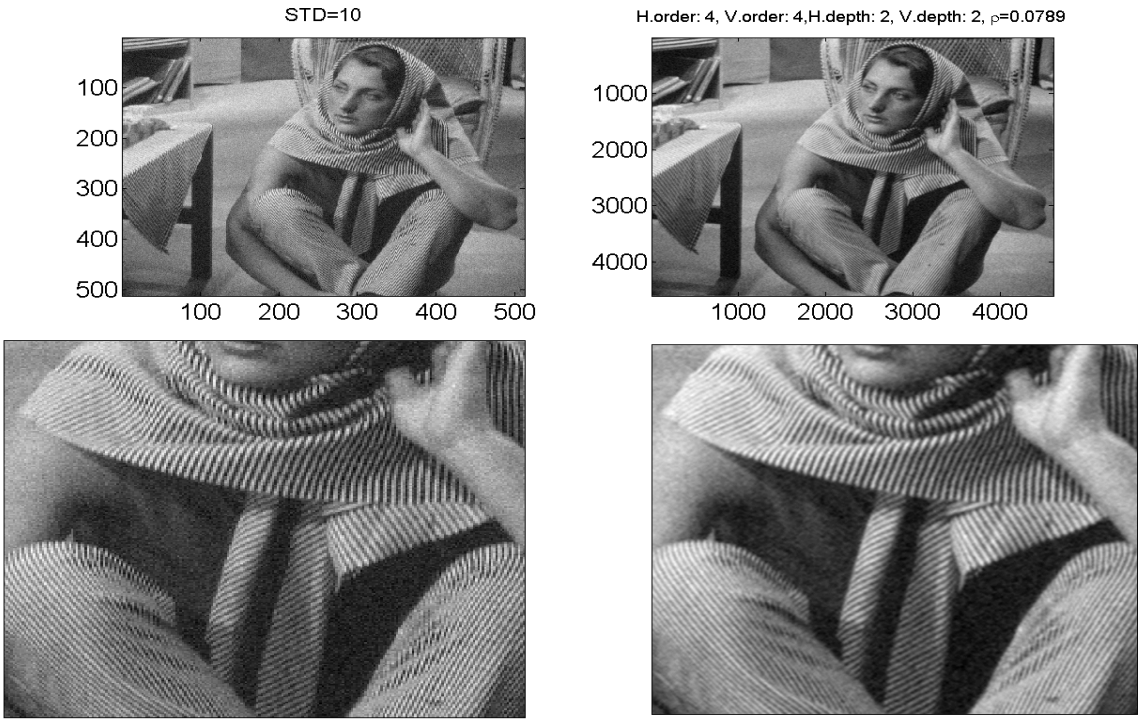

Figure 5.8: Left: Noised "Barbara" image in two formats. Top: The original image. Bottom: Fragment from the image. Right: The image upsampled by the smoothing splines $S_\rho^{4,4}(x,y)$ using the ternary subdivision in each direction.

5.3 The Prolate Spheroidal Wave Functions

We now use the Prolate Spheroidal Wave Functions (PSWFs) for rate change and compare its performance to splines. In this section, we review the needed concepts of the PSWFs that first appeared in [18].
Given a positive number c, we define the operator $F_c : L^2[-1,1] \to L^2[-1,1]$ such that

$$F_c[\psi](x) = \int_{-1}^{1} \psi(t) e^{icxt} dt. \tag{5.1}$$

Since F_c is compact, it has a discrete set of eigenvalues $\lambda_0, \lambda_1, \ldots, \lambda_n, \ldots$. Assume that they are ordered in a non-increasing order. Let ψ_n be the eigenfunction that corresponds to λ_n. For all integer $n \geq 0$ and for all real $-1 \leq x \leq 1$, $\lambda_n \psi_n(x) = \int_{-1}^{1} \psi_n(t) e^{icxt} dt$ holds.

We assume that the eigenvectors are normalized to length 1, that is $\|\psi_n\|_{L^2[-1,1]} = 1$ (as in [20, 1, 13]). The following theorem describes the eigenvalues and the eigenfunctions of F_c.

Theorem 5.1 ([18]) *Suppose that $c > 0$ is a real number, and that the operator F_c is defined by Eq. (5.1). Then, the eigenfunctions $\psi_0, \psi_1, \ldots$ of F_c are purely real, orthonormal and complete in $L^2[-1,1]$. The even-numbered functions are even, the odd-numbered ones are odd. Each function ψ_n has exactly n simple roots*

in $(-1,1)$*. All eigenvalues* λ_n *of* F_c *are non-zero and simple; the even-numbered ones are purely real and the odd-numbered ones are purely imaginary; in particular,* $\lambda_n = i^n |\lambda_n|$*.*

The operator $Q_c = \frac{c}{2\pi} F_c^* F_c$ has the same eigenfunctions as F_c and $Q_c[\psi](x) = \frac{1}{\pi}\int_{-1}^{1} \frac{\sin(c(x-t))}{x-t}\psi(t)dt$ where $Q_c[\psi]$ can be thought of as the output from a low pass filtering and its eigenvalues are $\mu_n = |\lambda_n|^2$. This intuitively links between PSWFs and band limited functions (in addition to being the eigenfunctions of the Fourier transform). The eigenvalues equation of Q_c is given by:

$$\int_{-1}^{1} \psi_n(x) \frac{\sin c(t-x)}{\pi(t-x)}\, dx = \mu_n \psi_n(t). \tag{5.2}$$

The solutions of Eq. (5.2) are denoted by $\psi_0(x), \psi_1(x), \psi_2(x), \ldots$ with the corresponding eigenvalues $\mu_0, \mu_1, \mu_2 \ldots$. The eigenvalues are ordered such that $\mu_0 > \mu_1 > \mu_2 \ldots$. Note that the PSWFs are the eigenfunctions of an ideal low pass filter operator and they form a basis for all bandlimited functions. We will use their basis property in the interpolation procedure. The ability of the PSWFs to approximate accuratly bandlimited functions has been recently investigated in [17].

Figure 5.9 shows the fast decay of the eigenvalues of F_c (in absolute value).

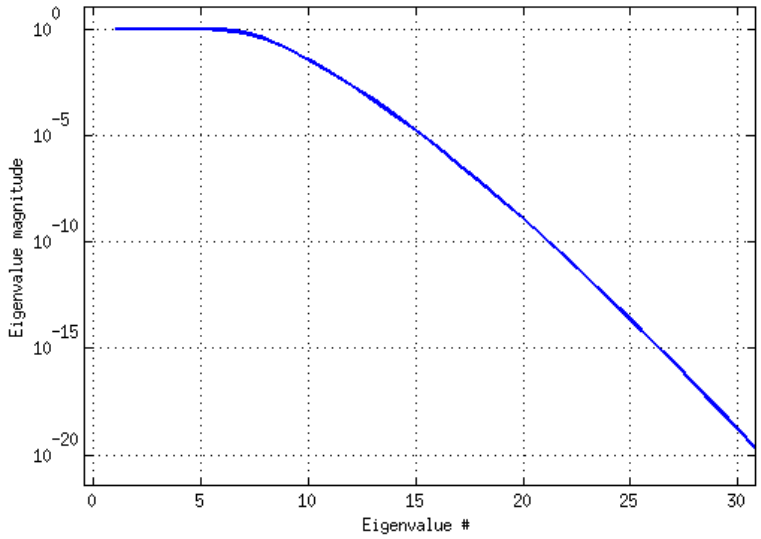

Figure 5.9: Eigenvalues of F_c in absolute value for $c = 10$

5.3.1 Problem Setup

Assume we are given a set of points $\{x_i\}_{i=1}^N$ on the interval $[-1,1]$ taken from a bandlimited function $f(x)$ with bandwidth c and an additional point z. We want to compute the weights $\{h_i\}_{i=1}^N$ that approximate $f(z)$ such that $\tilde{f}(z) = \sum_{i=1}^N h_i f(x_i)$. Moreover, we are looking for a solution that is independent of the actual value of the function $f(x)$ so it can be applied to any bandlimited function with bandwidth c. The weights

computation can be done by approximating a basis for the bandlimited functions. If the basis functions are approximated then we can find weights applicable to all the bandlimited functions (bandwidth c). Given bandwidth c, a set of points $\{x_i\}_{i=1}^N$ and a point z, we can solve the following least-squares (LS) problem by minimizing $\epsilon = \|e^{ic\omega z} - \sum_{i=1}^N h_i e^{ic\omega x_i}\|_2^2$ to compute the weights $\{h_i\}_{i=1}^N$.

Complex exponents are taken as basis functions since they are the eigenfunctions of Linear-Time-Invariant (LTI) systems. By computing the gradient of $\epsilon(\mathbf{h})$ and setting it to zero we get the following set of linear equations: $\frac{\partial \epsilon}{\partial h_m} = \langle e^{ic\omega z} - \sum_{i=1}^N h_i e^{ic\omega x_i}, h_m e^{ic\omega x_m}\rangle = 0$, $\langle e^{ic\omega z}, e^{ic\omega x_m}\rangle - \sum_{i=1}^N h_i \langle e^{ic\omega x_i}, e^{ic\omega x_m}\rangle = 0$ to obtain for $m = 1, ..., N$

$$\frac{\sin\, c(z - x_m)}{c(z - x_m)} - \sum_{i=1}^{N} h_i \frac{\sin\, c(x_i - x_m)}{c(x_i - x_m)} = 0. \tag{5.3}$$

Equation (5.3) represents an $N \times N$ system of equations $\mathbf{Ah} = \mathbf{b}$ where $a_{mn} = \frac{\sin\, c(x_m - x_n)}{c(x_m - x_n)}$ and $b_n = \frac{\sin\, c(z - x_n)}{c(z - x_n)}$. This system consists of sinc functions, which are known to be optimal for the interpolation of bandlimited functions. In practice, however, this method (Eq. 5.3) is far from being optimal due to the rapid growth of the condition number of $\mathbf{A}$. Hence, even for small number of samples and a low frequency signal the condition number is huge.

5.3.2 Interpolation using PSWFs

Since $f(x)$ is bandlimited, it can be represented as a linear combination of PSWFs $f(x) = c_1\psi_1(x) + c_2\psi_2(x) + \ldots + c_n\psi_n(x) + \ldots$. It takes a series of approximated length $M = O(c + log(c))$ to achieve a good approximation of the order of λ_{M+1} [17]. The eigenvalues decay as a function of c such that the first $c + log(c)$ eigenvalues are of order 1 and the others are very close to zero (Fig. 5.9). Since f can be approximated with PSWFs, it is possible to use the same basis approach as in Section 5.3.1 and interpolate the values of the PSWFs by finding the weights. It is known that sinc functions are optimal. Equation 5.3 can be reformulated in terms of PSWFs, mainting the theoretical optimality. The matrices $\mathbf{A} = \{a_{mn}\} = \frac{\sin\, c(x_m - x_n)}{c(x_m - x_n)}$ and $\mathbf{b} = \{b_n\} = \frac{\sin\, c(z - x_n)}{c(z - x_n)}$ can be factorized using a new matrix $\mathbf{C}$, which is not necessarily square, such that $\mathbf{A} = \mathbf{C^T C}$ and $\mathbf{b} = \mathbf{C^T \tilde{b}}$. By using the identity $\frac{\sin\, c(x_m - x_n)}{c(x_m - x_n)} = \sum_j |\lambda_j|^2 \psi_j^c(x_m)\psi_j^c(x_n)$ we get that the matrix $\mathbf{C}$ is $c_{mn} = |\lambda_m|\psi_m(x_n)$. Rewriting Eq. (5.3) in terms of the new matrix, we get

$$\mathbf{C^T C h} = \mathbf{C^T \tilde{b}} \tag{5.4}$$

which is the weighted LS solution of

$$\mathbf{C h} = \tilde{\mathbf{b}} \tag{5.5}$$

where $\tilde{b}_n = \psi_n(x_n)$. Explicitly, Eq. 5.5 it can written as:

$$\begin{aligned}
|\lambda_1|\psi_1(z) &= c_1|\lambda_1|\psi_1(x_1) + ... + c_N|\lambda_1|\psi_1(x_N) \\
|\lambda_2|\psi_2(z) &= c_1|\lambda_2|\psi_2(x_1) + ... + c_N|\lambda_2|\psi_2(x_N) \\
&\vdots \\
|\lambda_M|\psi_M(z) &= c_1|\lambda_M|\psi_M(x_1) + ... + c_N|\lambda_M|\psi_M(x_N),
\end{aligned}$$

Equation 5.5 has the same (least-squares) solution as Eq. (5.3), but its condition number is exactly the square root of the matrix in Eq. (5.3). It is shown in [15] that the obtained solution of Eq. (5.5) is very accurate despite the large condition number. In a nuteshell, given that the SVD of $\mathbf{C}$ by $\mathbf{U\Sigma V^T}$, then, the singular values of $\mathbf{C}$ are almost identical to the absolute value of the eigenvalues λ_i such that $\sigma_i(\mathbf{C}) = \mathcal{O}(|\lambda_i|)$ (see Figure 5.3.2) leading to a numerically stable equations as the left side is proportional with the right hand side which is dominated by $|\lambda_i|$. This "balance" provides an accurate numerical solution. A more rigorous analysis also requires to analyze the matrix $\mathbf{U}$ of the SVD as it can theoretically reorder the equations. A complete analysis appears in [15].

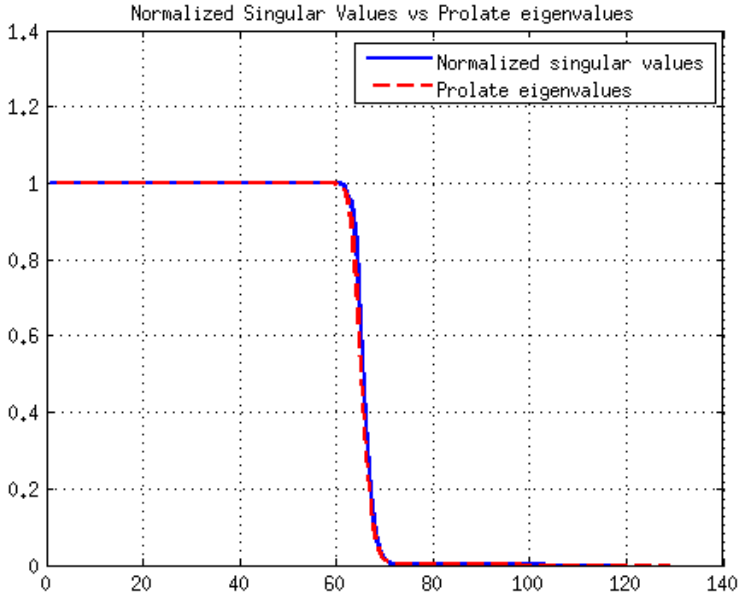

Figure 5.10: The singular values of $\mathbf{C}$ vs $|\lambda_i|$

Figure 5.3.2 shows the singular values of the matrix $\mathbf{C}$ with respect to the PSWF's eigenvalues which indicate that the equation can be solved accurately despite the large condition number.

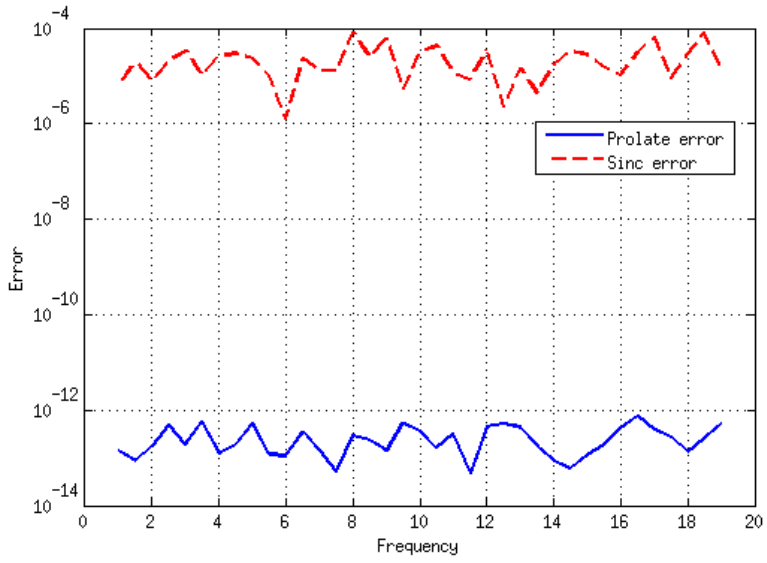

Figure 5.11: Error Comparison between Sinc and Prolate methods

Equation 5.5 was tested on a simple bandlimited function $f(x) = \cos(2\pi fx)$ where the number of samples is $N = 2f$. An even number of equispaced samples were taken on the interval $[-1, 1]$ and the interpolation goal was to reconstruct f at $x = 0$. Figure 5.11 compares between the numerical error obtained using sinc functions with the error obtained using PSWFs under identical conditions. Clearly, the numerical error obtained using PSWFs is smaller by a factor of 10^8.

The PSWF interpolation is done by the application of the interpolation scheme to each dimension separately. By assuming that both dimensions have the same bandwidth (same c is used) then the weights can be computed only once.

We now compare between the performances (three criteria) of splines of order 8 and PSWFs on digital images: visual quality (see Fig. 5.12), achieved PSNR and computational time (see both in Table 5.1).

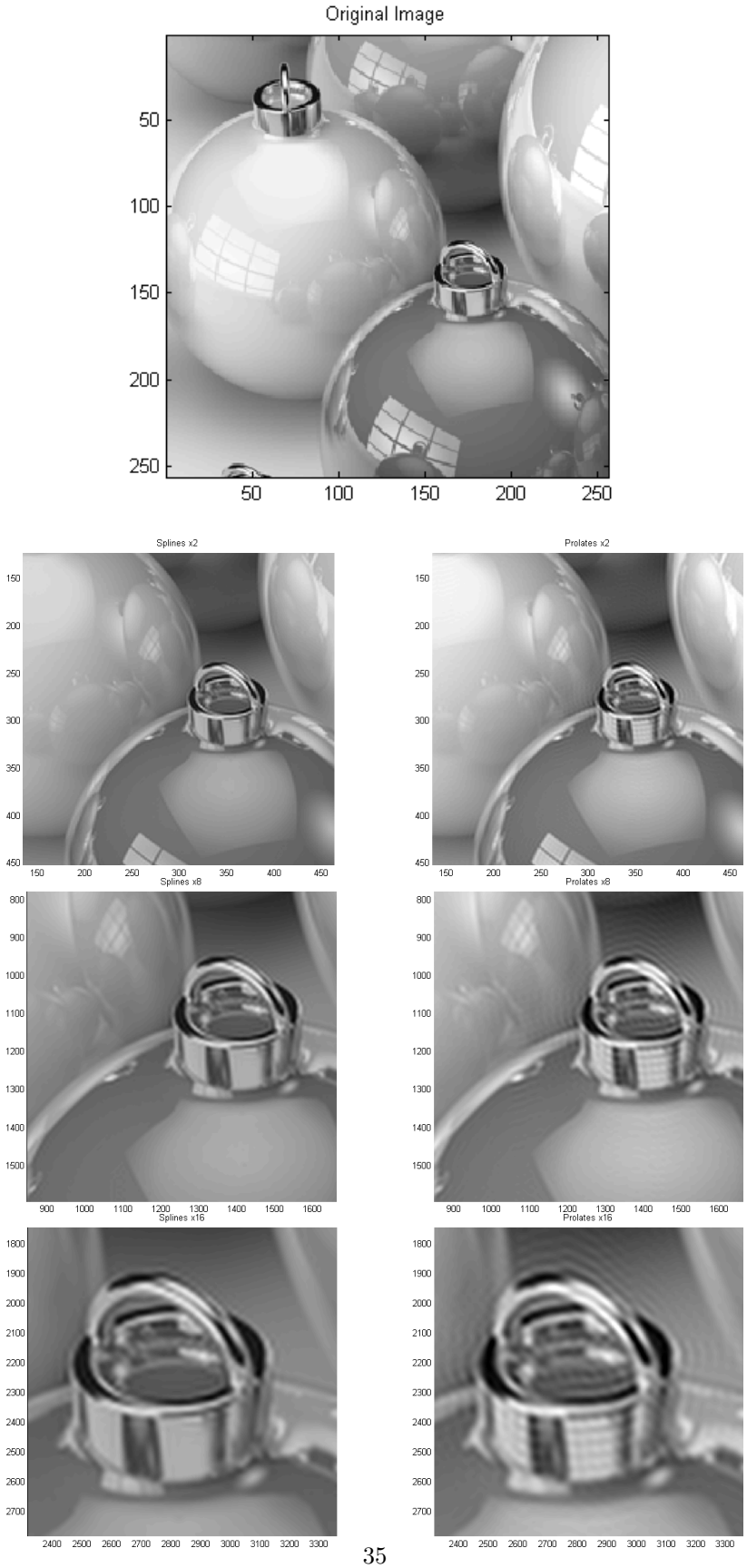

Figure 5.12: Comparison between the performance of spline of order 8 (left column) and prolate with $c = 280$ (right column)

We see that the splines produce better quality with less artifacts although the achieved PSNR (Table 5.1) are very similar.

Upsampling	PSWF PSNR	Spline PSNR	PSWF Time [sec]	Spline Time [sec]
2	28.7	29.2	24	0.05
4	24.7	24.4	41	0.2
8	22.1	21.8	80	0.8
16	20.5	20	150	3.4

Table 5.1: Performance comparison on the achieved PSNRs and on the processing time between splines of order 8 and prolates on the usampling by factor of 2, 8 and 16 of the source image in Fig. 5.12.

Conclusions

Splines tools appear in many important applications. Splines have been designed by their samples at grid points. We provide explicit designs of splines of any order to achieve fast calculation of their values at internal points between grid points. They are based on a fast and efficient scheme for computation of one- and multi-dimensional periodic splines of any order at triadic rational points and of splines of even order at dyadic rational points starting from their samples at equidistant grid points. We prove that if the spline order is even then the scheme at each step generates values of the initial spline. Thus, after m iterations the values $S(k/2^m)$ are derived. The calculations are reduced to those that come from the application of one direct and one inverse FFT independently of the number of iterations. We apply these constructions to devise algorithms for image restoration and for rate conversion to different sample rates. It also works well for noisy data. Upsampling of images by prolate spheroidal wave functions demonstrate one major application. Their performances are compared with splines.

Acknowledgement

The authors would like to thank Andrei Osipov and Vladimir Rokhlin from Yale University and Yoel Shkolnisky from Tel-Aviv University for fruitful discussions and for providing part of the PSWFs code.

References

[1] V. Rokhlin A. Osipov. On the evaluation of prolate spheroidal wave functions and associated quadrature rules. *Yale CS Technical Report #1471*, 2013.

[2] J. H. Ahlberg, E. N. Nilson, and J. L. Walsh. *The theory of splines and their applications.* Acad. Press, New York, 1967.

[3] A. Aldroubi, M. Unser, and M. Eden. Cardinal spline filters: stability and convergence to the ideal sinc interpolator. *Signal Processing*, 28(2):127–138, 1992.

[4] A. Averbuch and V. Zheludev. Spline-based deconvolution. *Signal Processing*, 89:1782–1797, 2009.

[5] A. Averbuch, V. Zheludev, G. Fatakhov, and E. Yakubov. A ternary interpolatory subdivision schemes originated from splines. *International Journal of Wavelets, Multiresolution and Information Processing*, 9(4):611–633, 2011.

[6] A. Averbuch, V. Zheludev, and M. Khazanovsky. Deconvolution by matching pursuit using spline wavelet packets dictionaries. *Applied and Comp. Harmonic Analysis*, 31:98–124, 2011.

[7] M. J. Bastiaans. Gabor expansion and the zak transform for continuous-time and discrete-time signals. In Y. Y. Zeevi and R. Coifman, editors, *Signal and image representation in combined spaces, 23–69, Wavelet Anal. Appl., 7*, pages 23–69, Academic Press, San Diego, CA, 1998.

[8] N. Dyn. *Tutorials on Multiresolution in Geometric Modelling*, chapter Analysis of convergence and smoothness by the formalism of Laurent polynomials, pages 51–68. Springer, 2002.

[9] N. Dyn, J. A. Gregory, and D. Levin. Analysis of uniform binary subdivision schemes for curve design. *Constr. Approx.*, 7:127–147, 1991.

[10] J. C. Holladay. Smoothest curve approximation. *Math. Tables Aids Comput.*, 11, 1957.

[11] Kwan Pyo Ko, Byung-Gook Lee, and Gang Joon Yoon. A ternary 4-point approximating subdivision scheme. *Applied Mathematics and Computation*, 190:1563–1573, 2007.

[12] N. Dodgson M. Sabin M. Hassan, I. Ivrissimitzis. An interpolating 4-point c^2 ternary stationary subdivision scheme. *CAGD*, 19(1):1–18, 2002.

[13] V. Rokhlin and H. Xiao. Approximate formulae for certain prolate spheroidal wave functions valid for large value of both order and band limit. *Applied and Computational Harmonic Analysis*, 22:105–123, 2007.

[14] I. J. Schoenberg. Spline functions and the problem of graduation. *Proc. Nat. Acad. Sci. USA*, 52:947–950, 1964.

[15] G. Shabat, Y. Shkolnisky, and A. Averbuch. High precision interpolation of band limited functions. *In preparation.*

[16] C.E. Shannon and W.Weaver. *The Mathematical Theory of Communication.* The University of Illinois Press, Urbana, IL, 1949.

[17] Y. Shkolnisky, M. Tygert, and V. Rokhlin. Approximation of bandlimited functions. *Applied and Computational Harmonic Analysis*, 21(3):413–420, 2006.

[18] D. Slepian and H. O. Pollak. Prolate spheroidal wave functions, Fourier analysis, and uncertainty - I. *Bell System Techincal J.*, pages 43–63, 1961.

[19] J. M. Whittaker. On a new method of graduation. *Proc. Edinburgh Math. Soc.*, 41:63–75, 1923.

[20] H. Xiao, V. Rokhlin, and N. Yarvin. Prolate spheroidal wave functions, quadrature and interpolation. *Inverse Problems*, 17(4):805–828, 2001.

[21] J. Zak. Finite translations in solid-state physics. *Phys. Rev. Lett.*, 19(4):1385–1387, 1967.

[22] V. A. Zheludev. Periodic splines, harmonic analysis, and wavelets. In Y. Y. Zeevi and R. Coifman, editors, *Signal and image representation in combined spaces*, Wavelet Anal. Appl., 7, pages 477–509. Academic Press, San Diego, CA,, 1998.

[23] V. A. Zheludev. Interpolatory subdivision schemes with infinite masks originated from splines. *Advances in Comp. Math.*, 25:475–506, 2006.